BIOPHYSICS

The conductance of KCNQ2 and its pathogenic variants is determined by individual subunit gating

Andy Hinojo-Perez[1]†, Jodene Eldstrom[2]†, Ying Dou[2], Allan Marinho-Alcara[1]‡, Michaela A. Edmond[1], Alicia de la Cruz[3]§, Marta E. Perez Rodriguez[3], Maykelis Diaz-Solares[1], Derek M. Dykxhoorn[4], David Fedida[2]*, Rene Barro-Soria[1]*

KCNQ2 channel subunits form part of the M-current and underlie one of the major potassium currents throughout the human nervous system, regulating resting membrane potentials, shaping action potentials, and impeding repetitive neuronal firing. However, how individual subunits within tetramers control channel functionality remains unresolved. Here, we investigate (i) whether opening of KCNQ2 channels requires a concerted step or can result from independent subunit activation and (ii) how individual subunits regulate gate opening and conductance. The E140R mutation in the S2 segment prevents activated voltage sensor conformations, but concatemeric constructs containing up to three E140R subunits retain KCNQ2-like currents. The underlying single-channel currents show subconductance levels resulting from limitations in inner gate dimensions, determined by the number of activated subunits and their spatial arrangement. Channel opening is allosteric and requires activation of only a single subunit, which can accentuate the influence of clinically relevant heterozygous mutations at threshold voltages.

INTRODUCTION

Potassium channels, including members of the voltage-gated potassium family Kv7.1 to Kv7.5, also known as KCNQ channels (*1*, *2*), play key inhibitory roles in excitable cells by dampening membrane excitability (*3*, *4*). The unique biophysical properties of KCNQ2 to KCNQ5 channels, including a hyperpolarized activation potential, slow activation and deactivation kinetics, and a lack of inactivation, allow these channels to regulate the membrane resting potential, shape action potential repolarization, and reduce repetitive neuronal burst firing (*3*, *5*, *6*). Mutations in KCNQ channels cause hyperexcitability-related disorders, including cardiac arrhythmias, pain, and epileptic encephalopathies linked to delayed psychomotor development and cognitive impairment comorbidities (*7*–*12*). While native neuronal KCNQ channels are mainly composed of heterotetrameric combinations of KCNQ2/3 (more recently also by KCNQ2/5 and KCNQ3/5 subunits) (*3*, *4*, *13*, *14*), homotetrameric assemblies of channel subunits (e.g., KCNQ2 channels) have also been shown to generate the M-current in neurons (*14*, *15*), particularly during early developmental stages (*16*, *17*). However, the contribution of each subunit to the overall functionality of the channel remains unknown. Answering this question is crucial to understanding the functional consequences of heterozygous channels that incorporate KCNQ subunits with clinically relevant pathogenic variants.

Recent cryo–transmission electron microscopy (cryo-EM) structures of KCNQ2 channels (*18*) show that similar to other Kv channels (*19*), KCNQ2 channels are tetrameric complexes with six transmembrane segments (S1 to S6) per subunit. The S5-S6 of the four subunits together form a centrally located pore domain that is flanked by the four voltage-sensing domains (VSDs), each composed of S1 to S4, oriented in a domain-swapped tetrameric architecture with the VSD of one subunit directly adjacent to the pore domain of a neighboring subunit. The C-terminal end of the S6 segments forms the gate (*20*), while the fourth transmembrane segment functions as the voltage sensor (VS) (*21*–*25*). In response to depolarization, the VSs move outward from their resting states to activated states that trigger channel opening and allow K^+ conductance (*26*). While crystallographic and cryo-EM high-resolution structural studies of KCNQ2 have provided detailed information about different channel domains in the activated/closed apo state or bound to different modulators, at present, they provide less information about dynamic changes in functional conformations that occur during voltage-dependent activation.

To understand how individual subunits work together and the impact that mutated subunits have on channel gating, it is important to assess the extent of the individual contribution of each subunit to the initiation of channel opening and the voltage-dependent characteristic of opening probability. Many voltage-gated K^+ channels require VS movements in multiple subunits to open the gate, as exemplified by the original Hodgkin and Huxley description of squid axon K^+ channel gating (*27*). This gating scheme, extended to other K^+ channels including Shaker and mammalian Kv channels, requires further concerted steps in the activation process to couple the rate of closed-state transitions with the rate of exponential current growth upon channel opening (*28*–*31*). The nature of these steps appears complex, with intersubunit interactions, especially between side chains of the S4-S5 linker and the distal S6 domains (*32*, *33*) seeming critical for the final cooperative gating transitions in both Shaker-like Kv channels and the archetypal Shaker channel itself (*34*, *35*).

[1]Department of Medicine, Miller School of Medicine, University of Miami, Miami, FL 33136, USA. [2]Department of Anesthesiology, Pharmacology and Therapeutics, University of British Columbia, Vancouver V6T 1Z3, Canada. [3]Department of Physiology and Biophysics, Miller School of Medicine, University of Miami, Miami, FL 33136, USA. [4]John P. Hussman Institute for Human Genomics, John T. Macdonald Foundation Department of Human Genetics, Miller School of Medicine, University of Miami, Miami, FL 33136, USA.
*Corresponding author. Email: david.fedida@ubc.ca (D.F.); rbarro@med.miami.edu (R.B.-S.)
†These authors contributed equally to this work.
‡Present address: Laboratory of Neurosciences and Electrophysiology, Brain Institute of Rio Grande do Sul, Pontifical Catholic University of Rio Grande do Sul, Porto Alegre, Brazil.
§Present address: Department of Biomedical and Clinical Sciences (BKV), Linköping University, SE-581 83 Linköping, Sweden.

Other channels like large conductance Ca^{2+}-activated K^+ channels (BK), hyperpolarization-activated cyclic nucleotide–gated K^+ and Na^+ channel 2 (HCN2), and KCNQ1 channels use different gating mechanisms that do not require multiple VS movements to open the gate (*36*–*41*). These channels show a constitutive conductance at negative voltages (*42*–*44*) that reflects a spontaneous fluctuation between closed and open states even in the absence of their respective ligands (*45*), and they operate as allosteric molecules where recruitment of additional activated VS in separate subunits favors subsequent gate opening. While KCNQ1 channels and the cardiac KCNQ1/KCNE1 channels that do not require activation of all four VSs to conduct (*36*, *46*) gate allosterically (*47*), little is known of other KCNQ− subfamily members, including neuronal KCNQ2 channels.

In this study, we investigate whether the opening of neuronal KCNQ2 channels requires a concerted movement of the VS in all four subunits or whether VS movement in a single subunit is sufficient to promote gate opening and K^+ conduction. We also determine how constraining the movement of VSs in different subunits affects the voltage dependence of channel opening and regulates channel conductance. We use the E140R mutation in the S2 segment of KCNQ2, in homomeric constructs, to restrict VS movement and to prevent activated conformations of individual channel subunits. We find that KCNQ2 channels do not require a concerted movement of all four subunits to open. Rather, channel opening can occur with activation of only a single VS, and patch clamp data and modeling indicate that recruitment of additional VSs does not facilitate further opening, suggesting an absence of positive allosteric coupling that is observed in other channels (*36*, *37*, *42*). Single-channel recordings of tetrameric channel assemblies containing different numbers of activatable VSs reveal notable subconductance states such that the larger the number of VSs restrained in the resting state (E140R), the smaller the unitary conductance of KCNQ2 channels. Understanding the dynamics and contribution of individual subunits to voltage-dependent gating may allow us to better predict pathological mechanisms of action with heterozygous mutations and consequently guide the development of precision therapy for KCNQ channelopathies.

RESULTS

Homomeric KCNQ2 channels bearing the E140R mutation are nonfunctional

In our previous study (*21*), we reported VS movement in KCNQ2 channels using the fluorescent probe Alexa Fluor 488 maleimide attached to the F192C site in the S3-S4 loop (hereafter, Q indicates a KCNQ2 subunit and Q* is the KCNQ2 subunit with the fluorescent probe attached), which indicated that the steady-state voltage dependence and the time course of VS movement closely correlated with channel opening/closing (*21*) (fig. S1). This close correlation between VS movement and activation gating suggests that unlike in many voltage-gated potassium channels, movement of multiple VSs is not required to open the KCNQ2 channel. Rather, in KCNQ2 channels, two alternatives might explain the close correlation in the time and voltage dependence of fluorescence and current: (i) one in which all four VS subunits move in a concerted manner to open the channel or (ii) one in which the movement of an individual VS might be sufficient to lead to pore opening.

To test the ability of individual VSs to facilitate activation gating in KCNQ2 channels, we designed plasmids in which we could control the subunit composition of the KCNQ2 channel by encoding concatemers of KCNQ2. These constructs contain different combinations of wild-type (wt) KCNQ2 subunits (referred to as Q) and immobile VSs that hold the E140R mutation (referred to as Q_i). The E140R mutation in the S2 segment of KCNQ2 is proposed to restrict VS movement via electrostatic repulsion, thereby preventing activated conformations (Fig. 1A) (*48*). We reasoned that if all four VSs must be activated to open the KCNQ2 channel gate, then channels bearing even one VS with restricted movement (i.e., containing the E140R mutation) will ensure that the channel remains closed. In contrast, if one VS in the activated state is sufficient for channel opening and all four VSs move independently from one another, then the presence of even one wt VS would permit channel function. wt KCNQ2 channels (Q) and channels containing the E140R mutation in all four KCNQ2 subunits (Q_i) were expressed in *Xenopus* oocytes and currents recorded using two-electrode voltage clamp (TEVC) electrophysiology (Fig. 1, A to C). Oocytes expressing the E140R channel produced negligible currents similar to those seen in the water-injected oocytes (Fig. 1, C and D), in agreement with a previous report (*48*). Despite the lack of current, biotinylation assays in oocytes detected similar levels of expression of the E140R channel and wt KCNQ2 at the plasma membrane (Fig. 1E and fig. S2 showing uncropped blot), suggesting that E140R did not interfere with trafficking. In addition, voltage clamp fluorometry (VCF) of channels comprised of four labeled E140R mutant subunits (Q_i*) showed no voltage-dependent fluorescence signals (Fig. 1, F and G).

The absence of voltage-dependent current and fluorescence signals from Q_i mutants suggests that the E140R mutation restrains VS in a nonactivated (down) position. Further support for this idea was obtained by testing the accessibility of the KCNQ2-F192C residue alone (Q*), and in the background of the E140R mutant (Q_i*), to extracellular tetramethyl-rhodamine C5-maleimide (TMRM) either in a low-K^+ "*N*-methyl-D-glucamine (NMDG)" or a high-K^+ solution (to keep the membrane at hyperpolarized or depolarized voltages, respectively; Fig. 1H). The rate of TMRM labeling of F192C (Q*) was almost twice as fast in the high-K^+ solution as in the NMDG solution (Fig. 1H, compare closed and open black circles). This suggests that the accessibility of residue F192C depends on the conformational state of the VS. In contrast, the rate of TMRM labeling of Q_i* was similarly slow in both depolarizing (high K^+) and hyperpolarizing (low K^+) solutions (Fig. 1H, compare closed and open red squares) with similar labeling rates seen for F192C (Q*) in the hyperpolarizing solution. Together, these data suggest that the VS likely remains in the down (resting) state in E140R (Q_i*) channels.

KCNQ2 channels bearing two E140R mutated VSs are functional

Tandem KCNQ2 dimers containing E140R and/or wt subunits were labeled with Alexa Fluor 488 at position F192C (*) (Fig. 2). Dimers containing one unlabeled and one labeled wt subunit (QQ*) produced channels with voltage-dependent fluorescence changes, $F(V)$, that correlated with the negatively shifted $F(V)$ relationship of channels with all four subunits labeled (Q*; Fig. 2D, dashed lines) (*21*) and $G(V)$ curves that were minimally right shifted compared to the $G(V)$ curve of Q* channels (Fig. 2, A and D, and Table 1). Note that the gating curve of labeled KCNQ2 (Q*) channels is left shifted compared with unlabeled wt KCNQ2 (Q) channels (Fig. 2, D and E,

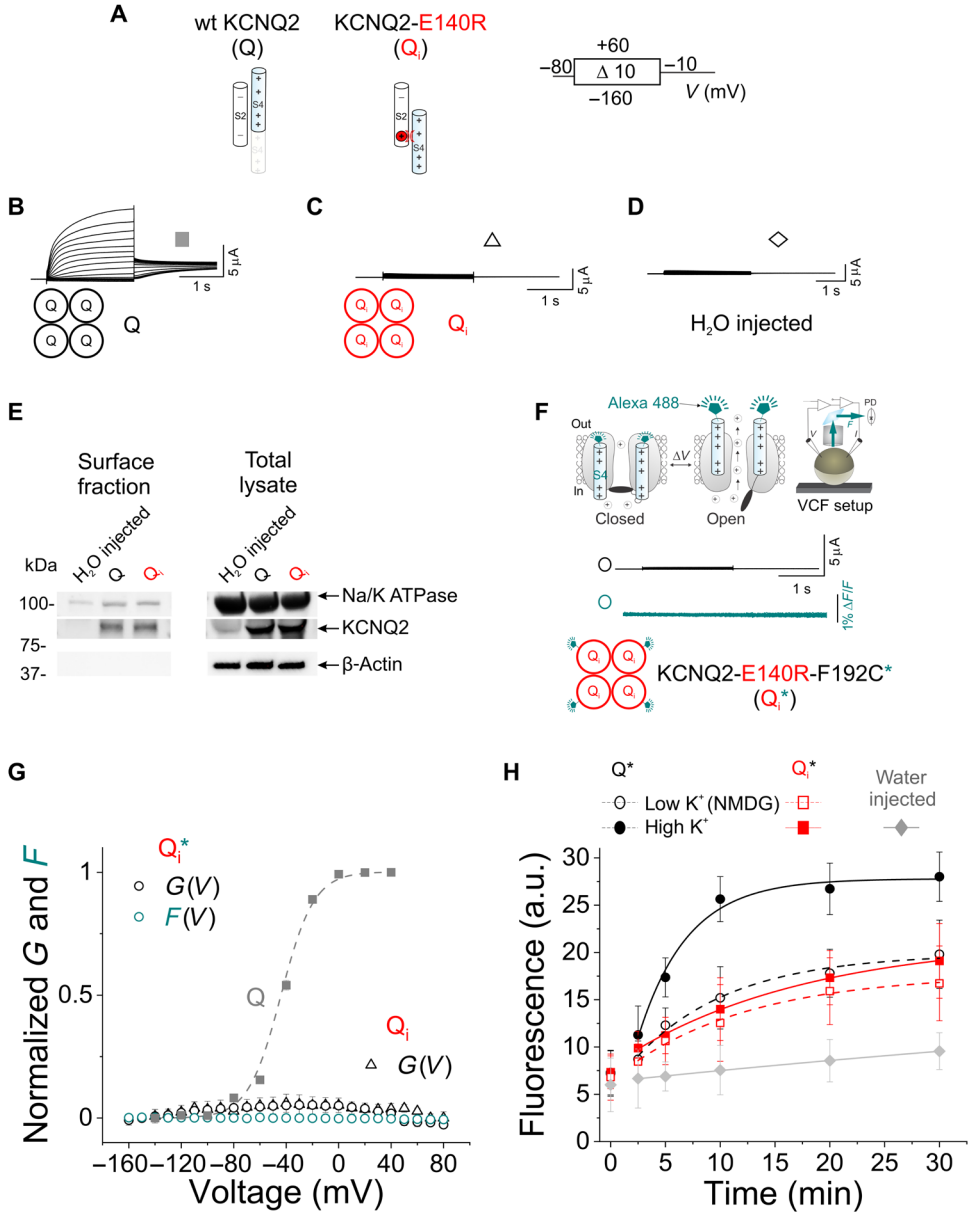

Fig. 1. The E140R mutation impairs KCNQ2 channel function. (**A**) Schematic of S4 activation in wt KCNQ2 (Q) channels and when the S4 movement is impeded by the E140R mutation (Q_i). (**B** to **D**) Current traces from oocytes expressing (B) wt KCNQ2 (Q) and (C) KCNQ2-E140R channels (Q_i) or (D) water-injected oocytes using the voltage protocol shown above. Sweep-to-sweep intervals were 15 s. (**E**) Western blot of surface fraction or total lysate extracted from water-injected oocytes and oocytes expressing Q and Q_i channels. The Na/K ATPase and β-actin are shown as controls. (**F**) Current (black) and fluorescence (cyan) traces from Alexa Fluor 488–labeled KCNQ2-E140R-F192C (Q_i*) channels using the voltage protocol in (A). Cartoons depict channel assemblies: wt KCNQ2 (Q, black circles), KCNQ2-E140R (Q_i, red circles), and Alexa Fluor 488–labeled KCNQ2-E140R-F192C (Q_i*, cyan cartoons attached to red circles). (**G**) Normalized $G(V)$ (black circles) and $F(V)$ (cyan circles) curves from Q_i* channels. Normalized $G(V)$ curves from Q (squares) and unlabeled Q_i (triangles) channels are shown for comparison. The midpoint of activation for the wt KCNQ2 (Q) fit is $GV_{1/2\,Q} = -41.7 \pm 1.9$ mV. Means ± SEM. $n = 8$ to 21. (**H**) TMRM labeling of water-injected oocytes (gray) and oocytes expressing the KCNQ2-F192C residue alone (Q*) and in E140R mutant (Q_i*) in high-K^+ and low-K^+ (NMDG) solutions. Data were fit with single exponentials, and labeling rates (k) were 3.7 ± 1.7 (Q* in high K^+), 2.2 ± 2.6 ($P = 0.04$) (Q* in NMDG), 1.8 ± 1.4 ($P = 0.01$) (Q_i* in high K^+), and 1.95 ± 1.85 fluorescence units/min ($P = 0.003$) (Q_i* in NMDG). Means ± SEM. P values indicate statistical difference from Q* in high-K^+ solution. P values are not different between Q* in low-K^+ (NMDG) solution and Q_i* in high-K^+ or low-K^+ (NMDG) solution. It was not possible to fit an exponential to water-injected oocyte data (gray). a.u., arbitrary units.

Table 1. Biophysical properties of single and concatemeric KCNQ2 constructs. Summary data for half-activation voltage ($V_{1/2}$) for each of $G(V)$ and $F(V)$ relationships and unitary conductance (g). *X. laevis*, HEKt (human embryonic kidney 293t cell line), tsA201 (transformed human kidney 293 cell line), and ltk (*ltk-* mouse fibroblasts). wt KCNQ2 subunit (Q), E140R subunit (Q_i), Alexa Fluor 488 maleimide–labeled F192C (Q*), and cysteine substitutions (Q^c). κ is the slope of the activation curve fitted with the Boltzmann equation (Eq. 2) (see Materials and Methods). Values are means ± SEM. n represents the number of cells analyzed. Statistical significance between $GV_{1/2}$, $FV_{1/2}$, and slope factors (k) was determined using a one-way ANOVA and a Bonferroni post hoc test ($P < 0.05$) compared with oocytes before application of MTSET and ($) compared with QQQQ in *X. laevis*, (&) compared with QQQQ in tsA201 cells, (@) compared with QQQQ in HEKt cells, and (#) compared with Q in *X. laevis*.

Construct	*n*	$GV_{1/2}$ (mV) (means ± SEM)	*Gk* (slope) (means ± SEM)	$FV_{1/2}$ (mV) (means ± SEM)	*Fk* (slope) (means ± SEM)	*g* (pS) (means ± SEM)	*p* $V_{1/2}$	Slope	
Q xenopus.l	21	−41.7 ± 1.9	11.1 ± 0.6	–	–	–	–	–	–
QQ xenopus.l	8	−41.0 ± 2.2	7.16 ± 0.8	–	–	–	–	–	–
Q* xenopus.l	10	−77.1 ± 2.7	14.0 ± 1.0	−87.1 ± 3.9	16.3 ± 0.8	–	–	–	–
QQ-R198Q xenopus.l	6	−58.5 ± 1.6	13.8 ± 1.5	–	–	–	0.007	0.025	#
QQ* xenopus.l	6	−74.4 ± 2.8	15.9 ± 2.0	−82.7 ± 2.9	13.1 ± 1.0	–	–	–	–
Q^*Q_i xenopus.l	3	−78.1 ± 5.1	15.3 ± 3.1	−86.4 ± 1.6	18.4 ± 2.1	–	0.65611/0.89	0.11793/0.093	G/F
QQ_i* xenopus.l	7	−51.9 ± 1.1	15.4 ± 1.0	–	–	–	0.0000281347/ ND	0.96181	G/F
Q^cQ^c before MTSET xenopus.l	7	−47.0 ± 1.3	13.4 ± 0.3	–	–	–	–	–	–
Q^cQ^c closed (+MTSET) xenopus.l	7	−44.9 ± 0.6	13.7 ± 0.6	–	–	–	1	–	Before MTSET
Q^cQ^c open (+MTSET) xenopus.l	7	−87.5 ± 1.5	14.7 ± 1.3	–	–	–	0.032	–	Before MTSET
Q^cQ_i before MTSET xenopus.l	5	−46.3 ± 2.5	12.3 ± 0.44	–	–	–	–	–	–
Q^cQ_i closed (+MTSET) xenopus.l	5	−44.4 ± 1.2	14.6 ± 0.47	–	–	–	0.990	–	Before MTSET
Q^cQ_i open (+MTSET) xenopus.l	5	−83.7 ± 1.1	14.4 ± 0.96	–	–	–	0.019	–	Before MTSET
QQ_i^c before MTSET xenopus.l	9	−39.0 ± 2.0	13.4 ± 1.8	–	–	–	–	–	–
QQ_i^c closed (+MTSET) xenopus.l	9	−36.9 ± 1.9	15.3 ± 0.9	–	–	–	0.973	–	Before MTSET
QQ_i^c open (+MTSET) xenopus.l	9	−37.8 ± 1.9	14.7 ± 1.8	–	–	–	0.371	–	Before MTSET
QQQQ xenopus.l	4	−32.8 ± 2.1	9.5 ± 0.5	–	–	–	–	–	–
QQ_iQQ xenopus.l	5	−34.9 ± 0.7	10.3 ± 0.6	–	–	–	1	0.9292	$
QQ_iQQ_i xenopus.l	4	−33.2 ± 6.3	8.8 ± 2.1	–	–	–	0.893	0.97574	$
$QQ_iQ_iQ_i$ xenopus.l	4	−33.5 ± 2.2	13.6 ± 0.8	–	–	–	0.999	0.37263	$
QQQQ tsA201	14	−24.5 ± 1.4	10 ± 0.5	–	–	–	–	–	–
QQ_iQQ tsA201	3	−26.3 ± 4.0	13.2 ± 1.6	–	–	–	0.993	0.134	&
QQ_iQQ_i tsA201	5	−29.1 ± 2.1	10 ± 1.3	–	–	–	0.699	>0.999	&

(*Continued*)

(*Continued*)

Construct	*n*	$GV_{1/2}$ (mV) (means ± SEM)	*Gk* (slope) (means ± SEM)	$FV_{1/2}$ (mV) (means ± SEM)	*Fk* (slope) (means ± SEM)	*g* (pS) (means ± SEM)	$p\,V_{1/2}$	Slope	
QQQ_iQ_i tsA201	3	−20.4 ± 3.3	12.0 ± 1.5	–	–	–	0.878	0.587	&
$QQ_iQ_iQ_i$ tsA201	13	−23.3 ± 2.4	10.3 ± 0.4	–	–	–	0.979	0.999	&
QQQQ HEKt	5	−24.4 ± 4.1	10.9 ± 2.6	–	–	–	–	–	–
QQQQ-R201C HEKt	6	−37.5 ± 4.8	11.9 ± 1.3	–	–	–	0.13615	0.96478	@
QQQQ-R214W HEKt	5	−18 ± 1.3	11.5 ± 0.7	–	–	–	0.77349	0.99332	@
$QQ_iQ_iQ_i$-R214W HEKt	4	−6.5 ± 5.8	10.2 ± 1.2	–	–	–	0.04784	0.99124	@
QQ_iQQ Itk	3–7	–	–	–	–	4.5 ± 0.3	–	–	–
QQ_iQQ_i Itk	3–7	–	–	–	–	1.7 ± 0.2	–	–	–
QQQ_iQ_i Itk	3–5	–	–	–	–	2.6 ± 0.1	–	–	–
$QQ_iQ_iQ_i$ Itk	3–5	–	–	–	–	1.6 ± 0.2	–	–	–
Q-F192S Itk	3–7	–	–	–	–	6.0 ± 0.4	–	–	–
Q^*Q_i Itk	3–6	–	–	–	–	1.3 ± 0.1	–	–	–
QQ_i^* Itk	3–7	–	–	–	–	1.5 ± 0.2	–	–	–
QQ Itk	3–6	–	–	–	–	6.0 ± 0.2	–	–	–

black dashed lines), as we have described in detail (*21*). Expression of dimers containing labeled wt and unlabeled E140R in different subunits (Q^*Q_i), which would produce tetramers having two labeled wt subunits and two unlabeled E140R subunits, displayed ionic currents and fluorescence signals similar to those from wt KCNQ2 channels containing only two labeled subunits (QQ*; Fig. 2, A and B, and Table 1). Notably, the $F(V)$ relationship of Q^*Q_i dimers closely correlated with its $G(V)$ curve and fell within the voltage-dependent range of $F(V)$ and $G(V)$ relationships of QQ* channels (Fig. 2, D and E, and Table 1). Expression of tandem dimers containing unlabeled wt and fluorescently labeled E140R in different subunits (QQ^*_i), which, when assembled as tetramers, will contain two Alexa Fluor–labeled VSs that are restrained in the resting state and two unlabeled wt KCNQ2 subunits, displayed negligible voltage-dependent fluorescence signals but produced currents with similar kinetics and midpoints of activation to wt KCNQ2 channels (both expressed as single Q and dimers QQ) (Fig. 2, C and F, and Table 1).

A second method was used to test functional VS activation and opening of mutant channel constructs containing heterogeneous VSs with the E140R mutation (Fig. 3). Previously (*21*), we mapped the extracellular excursion of VS residues during membrane depolarization in KCNQ2 channels using cysteine-scanning mutagenesis and state-dependent [2-(trimethylammonium)ethyl] methanethiosulfonate bromide (MTSET) modification approaches. We showed that external MTSET application modifies a stretch of ~9 amino acids, including the first gating charge (R198), in the open state but not in the closed state, which suggests that these residues move from a membrane-buried position in the resting state to the extracellular space during channel activation. MTSET modification and the appearance of ionic currents in cysteine-substituted residues of the VS can therefore be used to probe the VS movement and role of E140R-containing VSD when they are components of channels along with wt KCNQ2 subunits. In a similar manner to the KCNQ2 dimers used for VCF, we created two concatemeric constructs in which the R198C mutant (denoted as Q^c) was introduced either in adjacent subunits (Q^cQ_i) or in the same KCNQ2 subunits containing the E140R mutation (QQ_i^C), as is shown in the cartoons in Fig. 3A. Similar to our previous work (*21*), external application of 100 μM MTSET to oocytes expressing dimers of the R198C mutant (Q^cQ^c) increased the current amplitude, accelerated the kinetics of current activation, and left shifted the $G(V)$ relationship in the open state (at +20 mV) but not in the closed state (at −140 mV) (Fig. 3, A to D, top panels). These changes in gating properties upon MTSET application suggest that the R198 amino acid is not accessible in the closed state (with a resting-state VS) but becomes accessible in the open state (activated VS). Similarly, currents from oocytes expressing the Q^cQ_i dimer could be modified in the presence of 100 μM MTSET in a state-dependent manner, suggesting that the two R198C subunits (Q^c) could move from the resting to active state independent of the two restrained E140R subunits (Q_i; Fig. 3, A to D, middle panels). In contrast, application of 100 μM MTSET to oocytes expressing the QQ_i^C dimers resulted in no current changes in either the open or closed states (Fig. 3, A to D, bottom panels). The observation that QQ_i^C channels containing both the E140R and R198C mutations in the same subunit(s) are prevented from modification in the presence of MTSET shows that the E140R mutant truly restrains S4 movement. However, this restraint on movement imposed on the Q_i^C subunit does not prevent activation of the adjoined wt KCNQ2 subunits in the QQ_i^C channels. Oocytes expressing the QQ_i^C dimer exhibited ionic currents and $G(V)$ curves similar to those from oocytes expressing

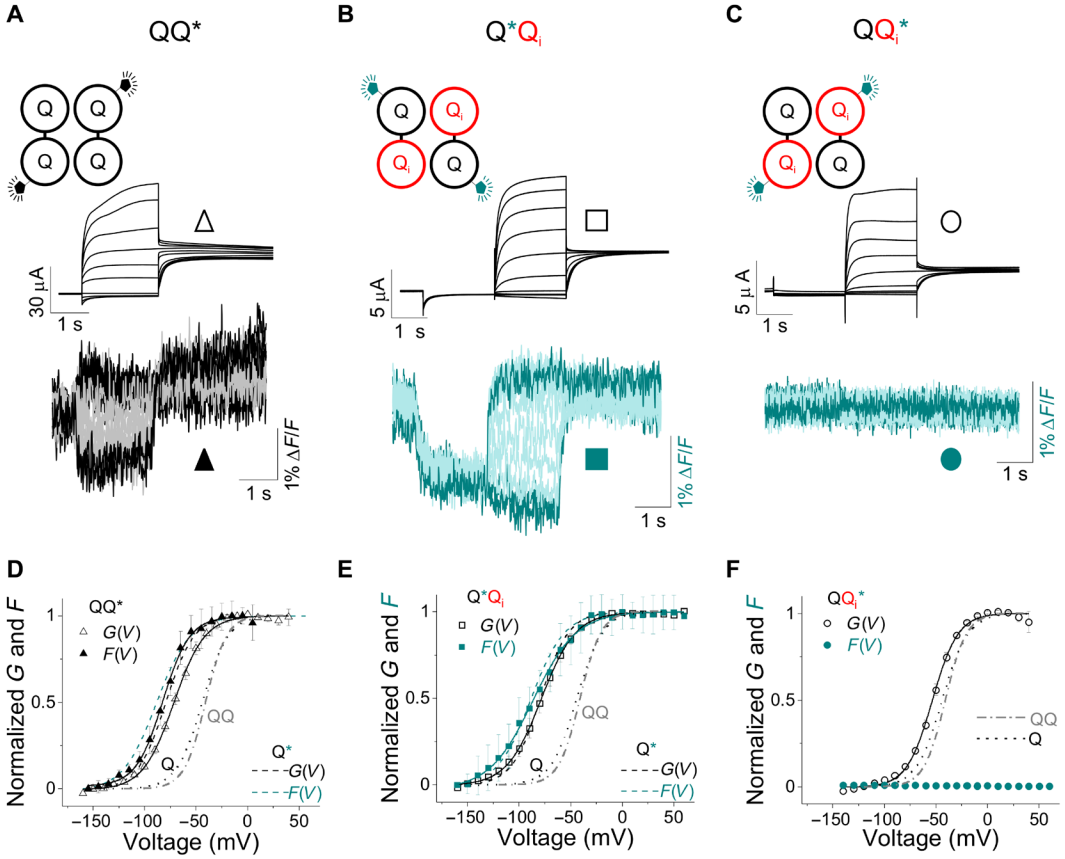

Fig. 2. KCNQ2 channels bearing two E140R mutations are functional. (**A** to **C**) Representative current (upper) and fluorescence (lower) traces from Alexa Fluor 488–labeled F192C (*) QQ* (triangles)–, Q*Q_i (squares)–, and QQ_i* (circles)–linked dimers for voltage steps between −160 and +60 mV in steps of 20 mV from a holding potential of −80 mV, followed by a −40-mV tail potential. In (B) and (C), a prepulse to −120 mV was used to deactivate the S4s more completely. Cartoons depict the channel assembly in the constructs: wt KCNQ2 subunit (Q, black circles), E140R subunit (Q_i, red circles), and Alexa Fluor 488 maleimide–labeled F192C (Q*, black or cyan cartoons attached to circles). Black lines between circles indicate tethers between subunits. (**D** to **F**) Normalized $G(V)$ (open symbols and solid line from a Boltzmann fit) and $F(V)$ (closed symbols and solid line from a Boltzmann fit) curves from labeled QQ* (triangles), Q*Q_i (squares), and QQ_i* (circles), respectively. In (D) to (F), dotted and dashed-dotted lines represent the $G(V)$ curves of single Q and dimers of QQ, respectively, for comparison. The midpoints of activation for the fits are as follows: $GV_{1/2\ QQ^*} = -74.4 \pm 2.8$ mV, $FV_{1/2\ QQ^*} = -82.7 \pm 2.9$ mV ($n = 6$), $GV_{1/2\ Q^*Q_i} = -78.1 \pm 5.1$ mV, $FV_{1/2\ Q^*Q_i} = -86.4 \pm 1.6$ mV ($n = 3$), $GV_{1/2\ QQ_i^*} = -59.1 \pm 1.1$ mV ($n = 7$), and $FV_{1/2\ QQ_i^*}$ = not determined; and $GV_{1/2\ Q} = -41.7 \pm 1.9$ mV ($n = 21$), $GV_{1/2\ QQ} = -41.0 \pm 2.2$ mV ($n = 8$), $GV_{1/2\ Q^*} = -77.1 \pm 2.7$ mV, and $FV_{1/2\ Q^*} = -87.1 \pm 3.9$ mV ($n = 10$; fig. S1) (shown in Table 1). Data represent means ± SEM.

wt KCNQ2 (Q) and dimeric (QQ) constructs (Fig. 3D, dotted and dashed lines, respectively). Collectively, the VCF and cysteine accessibility results on dimeric constructs indicate that KCNQ2 channel opening can occur in the presence of two E140R-containing subunits, and thus, channels can open with a minimum of two functional wt VSs.

Subunits with the E140R mutation are not excluded from channel assembly

The normal incorporation of subunits containing the E140R mutation into channel complexes was tested by assessing the sensitivity of channels to the channel blocker ML252 (fig. S3). Previous work has shown that compared to wt KCNQ2 channels (Q), the introduction of the mutation W236F (W/F) strongly attenuates the channel's sensitivity to ML252 (*49*). While 10 µM ML252 completely blocked the current from dimers of wt KCNQ2 channels (QQ-linked dimers), it only blocked QW/F dimers by ~5% (fig. S3, A to D and I, $n = 7$ to 8). Expression of dimers containing wt and W236F mutations in different subunits (QQW/F), which would produce tetramers having two wt and two W236F subunits, displayed a reduced sensitivity to ML252 (~50% reduction in peak current) compared to wt (QQ) (fig. S3, A, B, E, F, and I, $n = 6$). Application of 10 µM ML252 to dimers containing the E140R and W236F mutations in the same subunit linked to a wt subunit (QQ_iW/F), which would produce tetramers having two wt and two E140R-W236F subunits, exhibited similar ML252 sensitivity to that of QQW/F dimers (~45% reduction in peak current; fig. S3, G to I, $n = 5$). This result indicates that subunits containing the E140R mutation are not excluded from the channel complex during assembly and show identical ML252 responsiveness to wt subunits, which suggests a uniform population of expressed channels.

KCNQ2 channels open with a single activatable VS domain

To investigate the minimum number of VSDs required to open KCNQ2 channels, we produced concatemers of four KCNQ2 subunits containing variable numbers of VSs with the E140R mutation as shown in Fig. 4. These included constructs that were made up entirely of

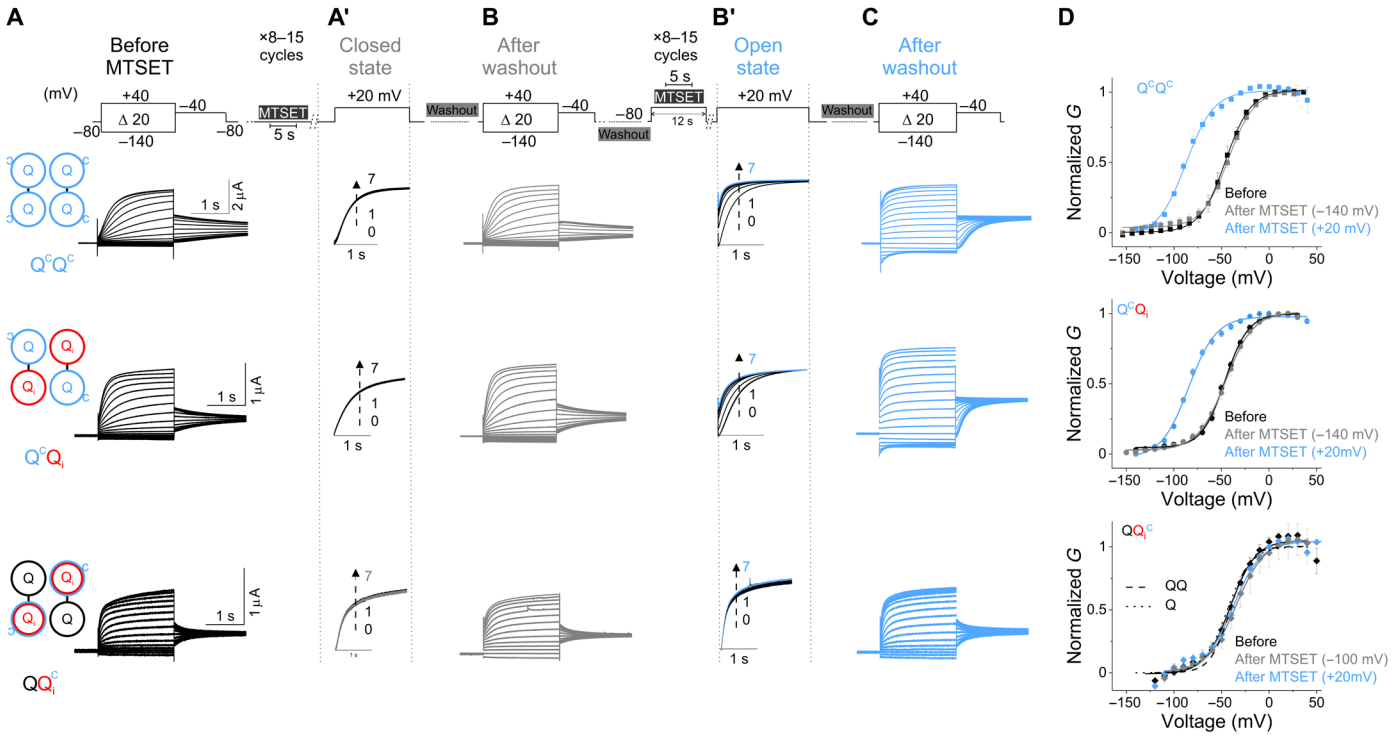

Fig. 3. State-dependent modification of Q^CQ_i-linked dimers by external MTSET is consistent with outward S4 motion in the R198C subunit (Q^C). KCNQ2-R198C Q^CQ^C (top), Q^CQ_i (middle), and $QQ_i{}^C$ (bottom) channel currents using the voltage protocol shown above (**A**) before and (**B** and **C**) after application of 100 μM MTSET in the (B) closed and (C) open states. MTSET is first applied ["closed state" in (**A**')] at −140 mV or −100 mV for 5 s in between 25-s washouts for 8 to 15 cycles, and the change in current is measured at +20 mV. On the same cell and after MTSET is washed out, MTSET is reapplied ["open state" in (**B**')] at +20 mV, as previously described in (*21*). (**D**) *G*(*V*) curves (lines from a Boltzmann fit) of (top) Q^CQ^C, (middle) Q^CQ_i, and (bottom) $QQ_i{}^C$ channels normalized to peak conductance before MTSET application (black). The *G*(*V*) relationships after MTSET application in the closed (gray) and open (blue) states are obtained from recordings of (B) and (C), respectively. The midpoints of current activation for the fits are as follows: $GV_{1/2\,Q^CQ^C\,\text{before}} = -47.0 \pm 1.3$ mV ($n = 7$), $GV_{1/2\,Q^CQ^C\,\text{closed}} = -44.9 \pm 0.6$ mV ($n = 7$), $GV_{1/2\,Q^CQ^C\,\text{open}} = -87.5 \pm 1.5$ mV ($n = 7$), $GV_{1/2\,Q^CQ_i\,\text{before}} = -46.3 \pm 2.5$ mV ($n = 5$), $GV_{1/2\,Q^CQ_i\,\text{closed}} = -44.4 \pm 1.2$ mV ($n = 5$), $GV_{1/2\,Q^CQ_i\,\text{open}} = -83.7 \pm 1.1$ mV ($n = 5$), $GV_{1/2\,QQ_i{}^C\,\text{before}} = -39.0 \pm 2.0$ mV ($n = 9$), $GV_{1/2\,QQ_i{}^C\,\text{closed}} = -36.9 \pm 1.9$ mV ($n = 9$), $GV_{1/2\,QQ_i{}^C\,\text{open}} = -37.8 \pm 1.9$ mV ($n = 9$), $GV_{1/2\,Q} = -41.7 \pm 1.9$ mV ($n = 21$), and $GV_{1/2\,QQ} = -41.0 \pm 2.2$ mV ($n = 8$; Table 1). Data represent means ± SEM.

wt KCNQ2 subunits (QQQQ), constructs containing one E140R (QQ_iQQ), two E140R (QQ_iQQ_i), or three E140R subunits ($QQ_iQ_iQ_i$). We expressed these tetramers in mammalian cells (i) because only two of the tetrameric constructs reliably expressed in oocytes (fig. S4), possibly due to the instability of the long-chain complementary RNAs of the tetramers, and (ii) to better compare whole-cell macroscopic currents with single-channel measurements obtained from mouse *ltk*− fibroblast cells (see Fig. 5). Expression of QQQQ tetrameric constructs in tsA201 (transformed human kidney 293 cell line) cells produced currents with steady-state conductance-voltage *G*(*V*) curves that were minimally right shifted compared to tetramers recorded in oocytes (Fig. 4, A and F, fig. S4, and Table 1). When compared to the wt tetrameric channels (QQQQ), we found that the other three E140R-bearing tetrameric channels, whether expressed in mammalian cells or oocytes, displayed no significant differences in their *G*(*V*) curves and slopes (Fig. 4F, fig. S4, and Table 1). Notably, while expression of QQQQ tetrameric constructs in tsA201 cells produced a larger current density than the $QQ_iQ_iQ_i$ mutant (fig. S5A), no differences in activation/deactivation kinetics or delay in channel activation was observed (fig. S5, B to D). Currents from the tetrameric constructs bearing one or three Q_i subunits were inhibited by the KCNQ2 channel blockers TEA (10 mM) or XE991 (30 μM) in both oocytes and mammalian cells (fig. S6), suggesting that the E140R mutation did not affect the tetrameric KCNQ2 architecture. To test whether the location of the E140R mutation within the tetrameric construct affected macroscopic currents, we also introduced two E140R subunits in adjacent positions within the tetramer (i.e., QQQ_iQ_i). The QQQ_iQ_i channels had a similar half-activation voltage ($GV_{1/2}$) to tetrameric channels in which the two E140R subunits are separated by a wt subunit (Fig. 4, C, D, and F, and Table 1), suggesting that the position of the E140R mutations within the tetramer does not substantially affect the voltage dependence of channel opening. Collectively, these data indicate that KCNQ2 channels can open even when only a single VS can activate.

E140R subunits reduce single-channel conductance

We next assessed the functional consequences of preventing one, two, or three VSDs from reaching activated conformations in KCNQ2 channels at the single-channel level. First, we measured the single-channel current of wt KCNQ2 channels using a tandem dimer (QQ) and found that QQ channels open with a maximal peak amplitude of 0.53 ± 0.02 pA at 0 mV (Fig. 5, A and B), as previously reported (*50*, *51*). We also tested the F192S mutant to see whether (and how) this would enhance expression as suggested by a previous report (*21*). Channels with F192S in each of the four subunits (Q^{F192S}) had the same single-channel current amplitude as wt QQ channels at

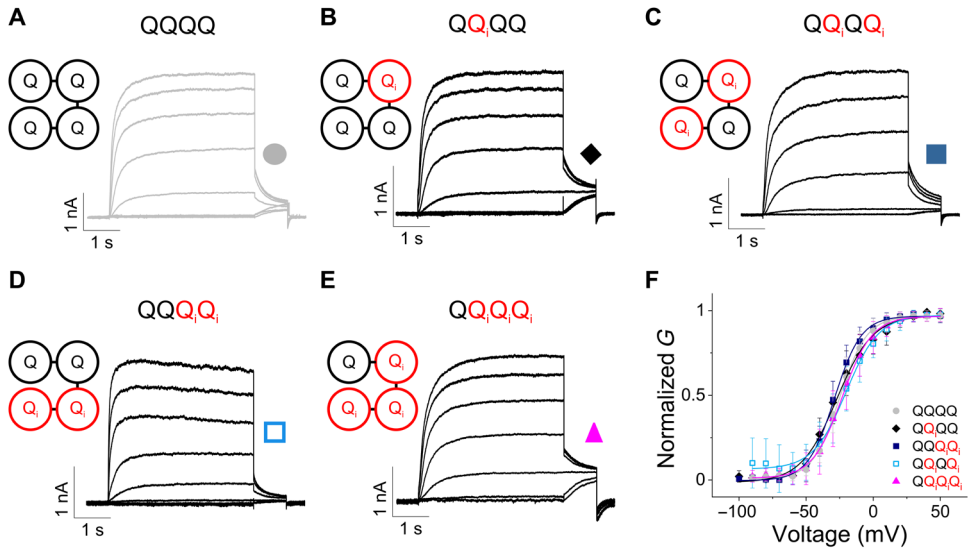

Fig. 4. Tetramers of KCNQ2 subunits containing one, two, or three E140R mutations produce currents. (**A** to **E**) Representative current traces from tsA201 cells expressing linked tetrameric channels as labeled for voltage steps between −100 and +60 mV in steps of 20 mV from a holding potential of −80 mV, followed by a −40-mV tail potential. Cartoons depict the channel assembly in the constructs: wt KCNQ2 subunit (Q, black circles) and KCNQ2-E140R subunit (red circles). Black lines in between circles indicate tethers between subunits. (**F**) Normalized $G(V)$ (solid line from a Boltzmann fit) curves from constructs shown in (A) to (E). The midpoints of activation for the fits are as follows: $GV_{1/2\ QQQQ} = -24.5 \pm 1.4$ mV ($n = 14$), $GV_{1/2\ QQ_iQQ} = -26.3 \pm 4.0$ mV ($n = 3$), $GV_{1/2\ QQ_iQQ_i} = -29.1 \pm 2.1$ mV ($n = 5$), $GV_{1/2\ QQQ_iQ_i} = -20.4 \pm 3.3$ mV ($n = 3$), $GV_{1/2\ QQ_iQ_iQ_i} = -23.0 \pm 2.4$ mV ($n = 13$); $P > 0.05$, one-way ANOVA and Tukey's post hoc test; see Table 1. Data represent means ± SEM.

0 mV (0.50 ± 0.02 pA; fig. S5) and were indistinguishable from wt at the single-channel level. Restraining either one, two, or three subunits from activation by including one, two, or three E140R mutated subunits led to a stepwise decrease in peak single-channel current. Thus, the currents from tandem constructs containing only one restrained subunit, QQ_iQQ, had smaller openings than QQ, 0.36 ± 0.01 pA at 0 mV (Fig. 5, A and B), but restraining an additional subunit (QQQ_iQ_i) further reduced the opening to 0.23 ± 0.003 pA. Last, the tandem construct with three E140R-containing subunits ($QQ_iQ_iQ_i$) had the smallest single-channel current amplitude of 0.126 ± 0.007 pA at 0 mV and openings became noticeably briefer.

To investigate the importance of opposing versus adjacent E140R-containing subunits, we also tested the QQ_iQQ_i construct and found that this configuration produced similarly small single-channel currents (0.133 ± 0.005 pA at 0 mV), as did channels made up of either three restrained VSs ($QQ_iQ_iQ_i$) or the dimers Q_iQ^* and QQ_i^* (Fig. 6, A to C, and fig. S7).

Markov kinetic models of KCNQ2 activation

The electrophysiological recordings from channel constructs with increased numbers of E140R mutant VSDs all showed robust currents, similar shape, and half-activation voltage $V_{1/2}$ (Fig. 4), which suggests that activation of a single VS is sufficient to open KCNQ2 channels. In addition, there appears little change in the shape or $V_{1/2}$ of the $G(V)$ relationships between the different Q* and Q_i constructs (Fig. 2). In formulating a model for KCNQ2 activation, the experiments suggest that a direct activation-to-opening pathway is required for each VS, and as there appears no energetic advantage in having more than one active VSD [$G(V)$ unchanged; Fig. 4F], positive allosteric regulation of the opening step once VSs are activated is not required. In our prior study of fluorescence from labeled KCNQ2-F192C (Q*) and mutant Q*-R198Q channels (*21*), it was difficult to separate more than one component of the fluorescence activation time course during VS activation and any further rearrangements upon pore opening that might change the fluorophore microenvironment could not be clearly defined, probably due to the similar voltage dependencies of the overall $F(V)$ and $G(V)$ relationships. However, the Q*-R198Q mutant seemed to better separate the first and second $F(V)$ components (*21*). Similarly, in related KCNQ1 channels, when the $G(V)$ and $F(V)$ relationships are separated widely by coexpression with KCNE1, a second, channel opening–related VS fluorescence component becomes apparent (*36*, *47*, *52*). In our KCNQ2 models, we included this second fluorescence component so that fluorescence associated with the horizontal VS transitions was denoted F1 and that associated with the opening transition F2.

These experimentally defined properties are reflected in model schemes and transition rate constants shown in Fig. 7A for labeled KCNQ2-F192C (Q*) channels, for dimers of Q^*Q_i, and tetrameric constructs of KCNQ2 where three of the four subunits contain the E140R mutation (Q_i) and only one activatable Q* subunit remains ($Q^*Q_iQ_iQ_i$). Fits to the fluorescence activation time course and steady-state fluorescence-voltage, $F(V)$, relationships of Q* (fig. S1) (*21*) were used to derive exponential relationships versus voltage for α and β (see Materials and Methods, Eq. 1) and obtain rate constants for horizontal model transitions, which define independent VS activation kinetics (see Materials and Methods). The α and β rate constants were then incorporated into a computer model of Q* to optimize δ and γ opening/closing transition rate constants (Fig. 7A) via iterative minimization of differences to Q* $G(V)$ and $F(V)$ experimental data (fig. S1).

Rate constants were used to generate steady-state $G(V)$ and $F(V)$ relationships for comparison with the experimental data (symbols in Fig. 7B) and model current and fluorescence waveforms (Fig. 7C).

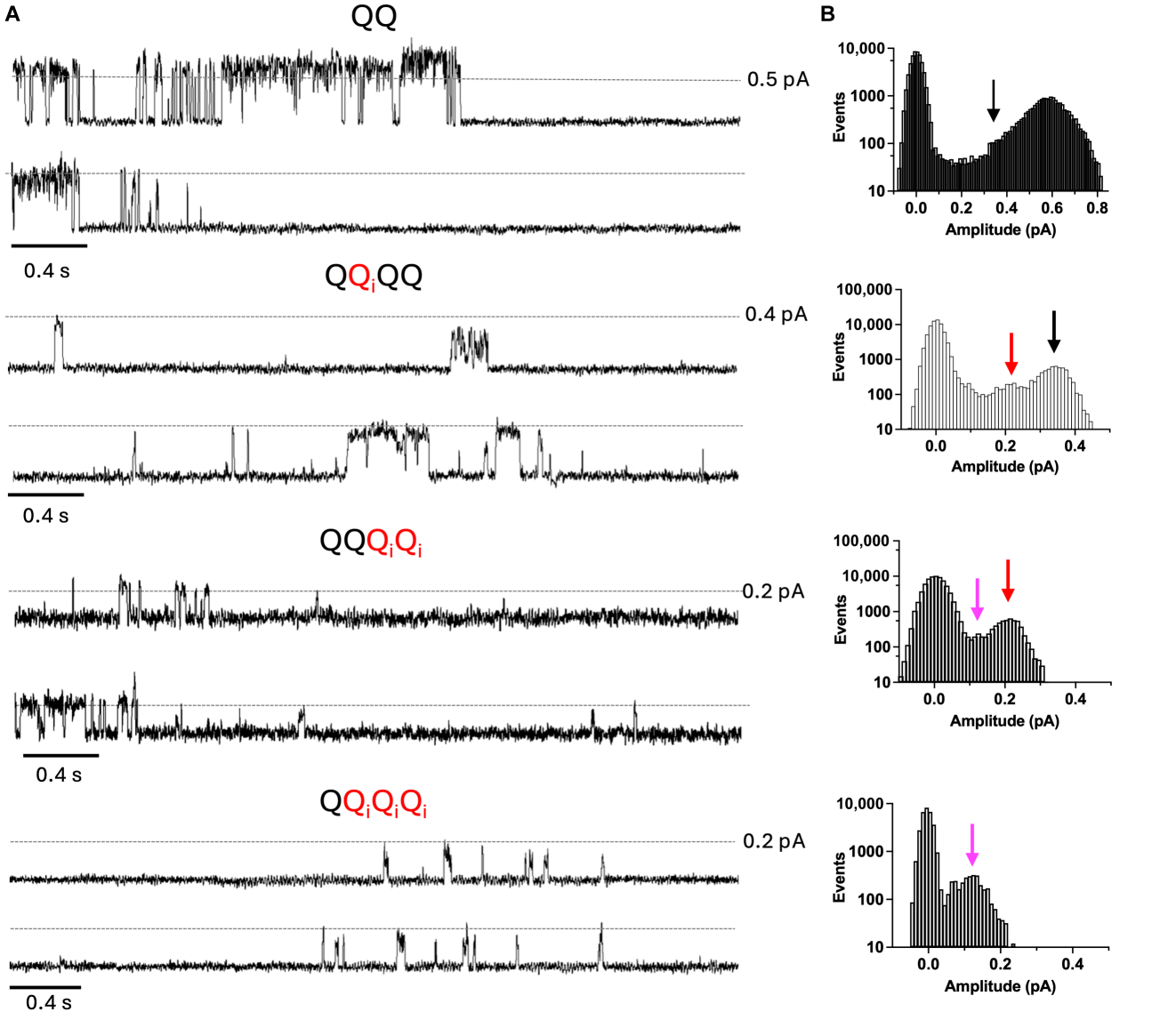

Fig. 5. Increasing the number of E140R-containing subunits in the channel complex reduces single-channel conductance. (**A**) Representative single-channel recordings of various KCNQ2 constructs as labeled above each set of records. Records are from the 0-mV test pulse portion of a protocol in which the patch was held at a holding potential of −80 mV and pulsed to 0 mV for 4 or 10 s ($QQ_iQ_iQ_i$ only) and then to −40 mV for 0.9 s, with an interpulse interval of 10 or 15 s. (**B**) All-points amplitude histograms of the traces shown in (A). The bin size for the histograms was 0.01 pA, and the *y* axis is shown as a log scale. The nonzero peaks were 0.57 pA for QQ, 0.34 pA for QQ_iQQ, 0.21 pA for QQQ_iQ_i, and 0.12 pA for $QQ_iQ_iQ_i$. Arrows highlight peaks representing subconducting states.

The $G(V)$ relations for the Q* models overlay each other and fit the experimental relationship closely. The $F(V)$ relationships for models that contain increasing numbers of Q_i subunits are shallower and diverge from each other at the foot of the curves, as expected from the rate constant multipliers in each model that define the speed of horizontal transitions. Notably, as for the $G(V)$s, the model $F(V)$ relationship fits the Q* $F(V)$ experimental data points well (Figs. 2D and 7B and fig. S1). When the relationships are replotted on a semi-log scale, it can be seen how well the models fit experimental data at very low open probabilities, a region where the α and β rate constants determined from fluorescence tracings are uncontaminated by fluorescence from opening transitions (Fig. 7D). The contribution of F1 and F2 to the overall $F(V)$ relationship for Q* is shown in Fig. 7E. It can be seen that F1 and F2 share a very similar voltage dependence and that the simulated F2 comprises about 25% of the total fluorescence at 0 mV.

Gating effects of individual subunits containing disease-causing mutations

Next, we investigated the functional gating of KCNQ2 channels bearing disease-associated gain-of-function (GOF) and loss-of-function (LOF) mutant subunits. If KCNQ2 channels can open when a single VS can activate, then in channels made up of heterogeneous subunits, the shape of the $G(V)$ relationship and half-activation voltage ($V_{1/2}$) will be affected by VS displaying different activation voltage dependencies. Thus, channels containing three wt subunits and one mutated subunit with a hyperpolarized $V_{1/2}$ (i.e., a GOF gating mutation) will open at voltages more hyperpolarized than channels entirely made up

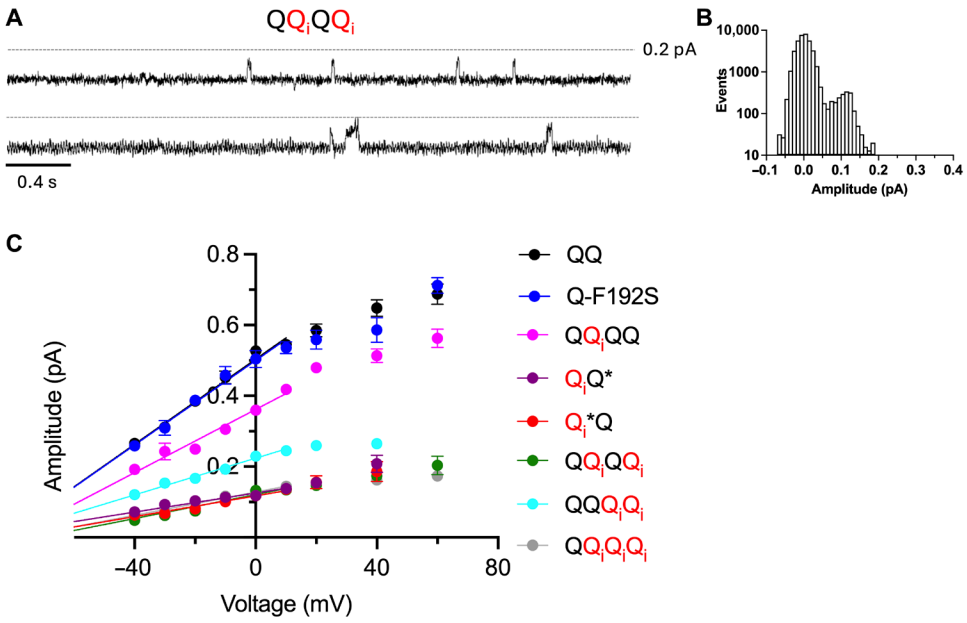

Fig. 6. Having two E140R-containing subunits across from one another reduces conductance to a level of construct containing three E140R subunits. (**A**) Representative single-channel records of QQ_iQQ_i. Records are from the 0-mV test pulse portion of a protocol in which the patch was held at a holding potential of −80 mV and pulsed to 0 mV for 4 s and then to −40 mV for 0.9 s, with an interpulse interval of 10 s. (**B**) All-points amplitude histograms of the traces shown in (A). The bin size for the histogram was 0.01 pA, and the *y* axis is shown as a log scale. The nonzero peak was 0.11 pA. (**C**) Unitary current amplitude-voltage curves for each of the dimer and tetramer constructs studied. Conductances were 6.0 ± 0.2 pS for QQ (n = 3 to 6), 6.0 ± 0.4 pS for Q-F192S (n = 3 to 7), 4.5 ± 0.3 pS for QQ_iQQ (n = 3 to 7), 2.6 ± 0.1 pS for QQQ_iQ_i (n = 3 to 5), 1.7 ± 0.2 pS for QQ_iQQ_i (n = 3 to 7), 1.3 ± 0.1 pS for Q_iQ^* (n = 3 to 4), 1.5 ± 0.2 pS for $Q_i{}^*Q$ (n = 3 to 7), and 1.6 ± 0.2 pS for $QQ_iQ_iQ_i$ (n = 3 to 5); see Table 1.

of wt subunits, whereas channels containing three wt subunits and one mutated subunit with a depolarized $V_{1/2}$ (i.e., LOF gating mutation) will open at a similar $V_{1/2}$ to wt channels but should show saturation of conductance at more positive potentials. To test this, we produced tetrameric KCNQ2 constructs made up of three wt (Q) subunits and either the GOF mutation [R201C (*53*, *54*), $QQQQ_{R201C}$] or the LOF mutation [R214W (*21*, *55*), $QQQQ_{R214W}$] (Fig. 8).

Consistent with a GOF gating phenotype (*54*), expression of $QQQQ_{R201C}$ tetramers produced currents with voltage-independent (around 20% remained open at negative voltages) and voltage-dependent components and a $V_{1/2}$ more hyperpolarized than wt QQQQ channels (Fig. 8, A, B, and E, and Table 1). Similarly, KCNQ2 dimers containing the severe GOF R198Q (*56*) in one subunit (QQ_{R198Q}) displayed hyperpolarized $V_{1/2}$ values and an elevated foot of the $G(V)$ curve compared to wt QQ channels (fig. S8). In contrast, the $V_{1/2}$ of $QQQQ_{R214W}$ channels was only minimally depolarized compared to those of wt QQQQ tetramers (Fig. 8, C and E, and Table 1), as the $QQQQ_{R214W}$'s $V_{1/2}$ remained largely governed by most wt subunits in the presence of the single LOF R214W subunit. Notably, currents from tetrameric constructs bearing the R214W mutation and three inhibitory E140R subunits, to restrict VS movement in all but the R214W subunit ($Q_iQ_iQ_iQ_{R214W}$), displayed more depolarized $V_{1/2}$ values than wt QQQQ channels (Fig. 8, D and E, and Table 1), since the $Q_iQ_iQ_iQ_{R214W}$'s voltage dependence of opening was solely governed by the LOF R214W phenotype.

DISCUSSION

Activation of a single VSD can open KCNQ2 channels

Knowledge of the detailed voltage-sensing mechanisms by which KCNQ2 gates has the potential to improve our understanding of how disease-causing mutations disrupt channel function. However, the kinetics and voltage-dependent contribution of individual VSD transitions to the overall channel gating have remained poorly described, in part, because of technical limitations in examining individual VS rearrangements and the use of coexpression systems that mask individual subunit function. In the current study, we overcame these challenges by using concatenated dimeric and tetrameric constructs containing different numbers of the E140R mutation in the S2 domain, previously shown to prevent VSs from reaching activated conformations (*48*), to control the number of activatable VSs and assess the impact on channel gating. Incorporation of E140R into all four subunits produced nonconducting channels despite surface membrane localization (Fig. 1), likely due to electrostatic clashes with positive charges in the S4 domain of the VS (*48*) that prevent channel activation and thus, gate opening. Constraining all four KCNQ2 subunits in the tetrameric channel (all four VSDs containing E140R, Q_i) abolished VS movement as measured by loss of VCF signals. Thus, by incorporating the E140R variant in the S2 transmembrane domain, we were able to constrain VS movement in KCNQ2 channels in a targeted manner.

With concatenated constructs, we tracked VS movement (fluorescence) in tandem dimers containing mixed wt and E140R VSs and correlated this with channel opening (ionic current). We found that labeled VS (*), either in the same (QQ^*_i) or opposite subunits (Q^*Q_i) to the E140R mutation, produces robust KCNQ2-like currents, but voltage-dependent fluorescence indicative of VS movement is only detected in those channels containing labeled wt subunits (Q^*Q_i), consistent with the E140R mutation preventing the E140R-VSs from reaching the activated state (Fig. 2). In addition, while Q^*Q_i and QQ^*_i channels had midpoints of current activation—$GV_{1/2}$—that

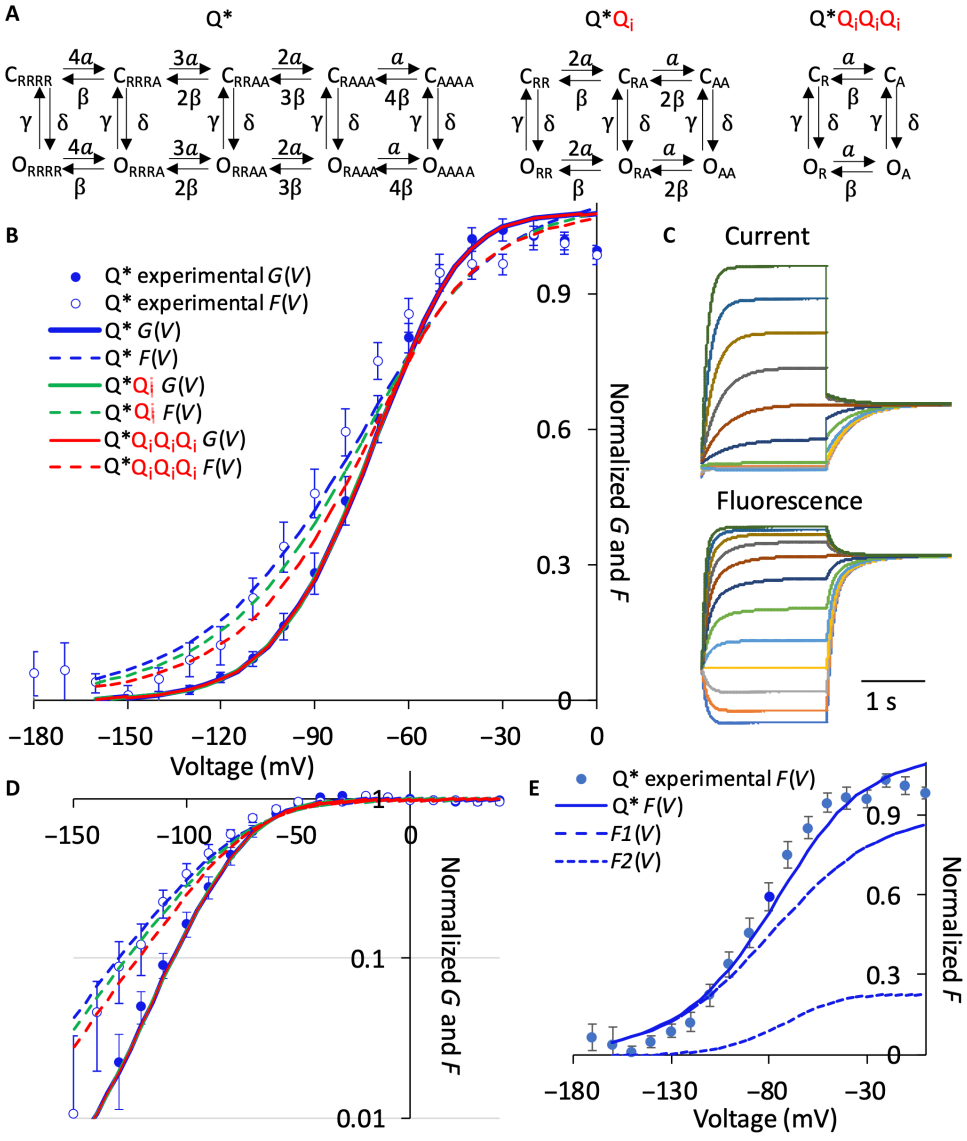

Fig. 7. Models of KCNQ2 activation. (**A**) Model schemes for labeled KCNQ2-F192C (Q*) and for channels with two E140R (Q*Q_i) and three E140R-containing ($QQ_iQ_iQ_i$) nonactivatable VSs. (**B**) $G(V)$ and $F(V)$ relations for the three models as indicated. Model $G(V)$s as solid lines overlay each other; $F(V)$s are dashed lines. Experimental Q* $G(V)$ data are shown as filled circles and $F(V)$ data as open circles. (**C**) For current and fluorescence tracings, the model protocol was as follows: *Vh* −120, 2 s to between −180 and +40 mV, step to −40 mV for 2 s. (**D**) $G(V)$ and $F(V)$ relations on a semilog plot, legend as for (B). (**E**) KCNQ2-F192C total fluorescence-voltage relation (Q*) and components *F1*(*V*) and *F2*(*V*). The $V_{1/2}$ and *k* values for the overall model *Q* F*(*V*) are −80.5 and 22.9 mV, respectively. For *F1*(*V*), $V_{1/2}$ and *k* values are −82.9 and 25.2 mV, and for *F2*(*V*), $V_{1/2}$ and *k* values are −73.4 and 14.4 mV, respectively. See Materials and Methods for rate constants.

followed their respective $GV_{1/2}$ of homomeric labeled Q* and unlabeled wt channels (Fig. 2 and fig. S1) (*21*), QQ* channels exhibited $GV_{1/2}$ values that were slightly more depolarized than those of labeled channels and unlabeled channels, suggesting that VS movements of freely movable wt subunits are independent. Cysteine accessibility experiments were used to verify our VCF results. Since MTSET modified channels containing the R198C probe (Q^c) in a state-dependent manner only if the mutation is expressed in the opposing subunit from E140R (QcQ_i) (Fig. 3), we concluded that R198C-VSD, but not E140R-VSD within the heterogeneous VS channel assembly, can move from the resting (membrane buried) unmodified state to an activated (extracellular space) modifiable state. Regardless of the positioning of the R198C probe, either in the same or opposite subunit as the E140R mutation, both Q^cQ_i and QQ^c_i channels produce measurable currents, as if the wt (Q) and wt-like VSDs (Q^c) move independently from the restrained E140R (Q_i)–bearing subunits. Lastly, whole-cell (Fig. 4) and single-channel recordings (Figs. 5 and 6) from heterogeneous channels containing as many as three VSDs restrained in the resting state and only one activatable VSD subunit ($QQ_iQ_iQ_i$) show that the channel can conduct.

These findings are in agreement with a body of data from KCNQ1 channels. Meisel and colleagues (*57*) used thermodynamic mutant cycle analysis of GOF and reduced-function KCNQ1 S4 mutations placed in one, two, three, or four S4 domains to show that the

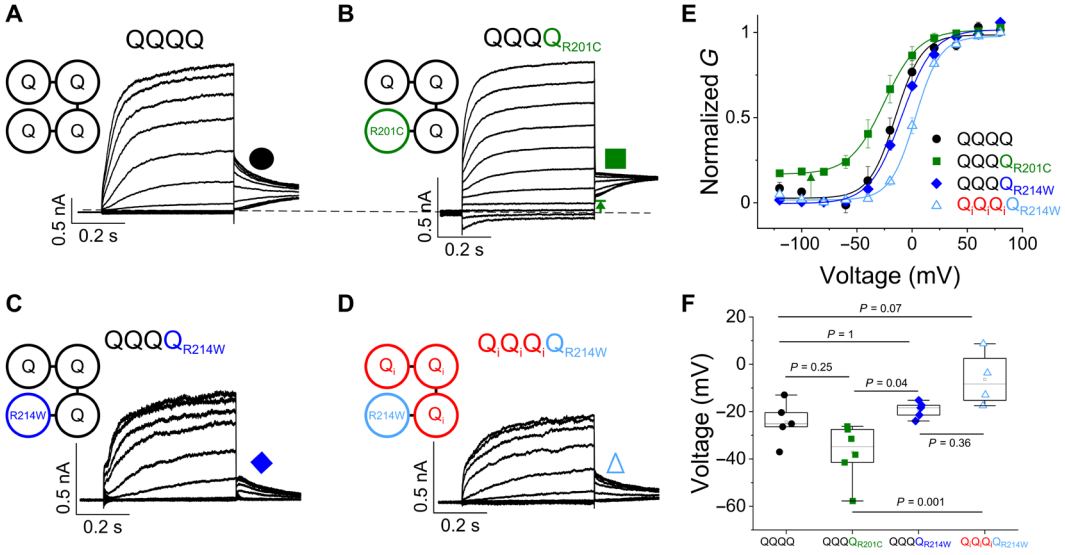

Fig. 8. The opening of heterozygous channels containing GOF or LOF mutations is controlled by the subunit displaying the strongest hyperpolarized $V_{1/2}$. (**A** to **D**) Representative current traces from cells expressing tetrameric constructs as labeled for voltage steps between −120 and +80 mV in steps of 20 mV from a holding potential of −80 mV, followed by a −40-mV tail potential. Cartoons depict the channel assembly in the constructs: wt KCNQ2 subunit (Q, black circles), KCNQ2-R201C subunit (green circles), KCNQ2-R214W subunit (blue circles), and KCNQ2-E140R subunit (red circles). Black lines in between circles indicate tethers between subunits. (**E**) Normalized $G(V)$ (solid line from a Boltzmann fit) curves from constructs shown in (A) to (D). (**F**) Summary data for $G(V)$ midpoints using Boltzmann fits from (E). The midpoints of activation for the fits are as follows: $GV_{1/2\ QQQQ} = -24.4 \pm 4.1$ mV ($n = 5$), $GV_{1/2\ QQQQ_{R201C}} = -37.5 \pm 4.8$ mV ($n = 6$), $GV_{1/2\ QQQQ_{R214W}} = -18.0 \pm 1.3$ mV ($n = 5$), $GV_{1/2\ Q_iQ_iQ_iQ_{R214W}} = -6.5 \pm 5.8$ mV ($n = 4$); see Table 1. Data represent means ± SEM.

movement of individual VSs contributed sequentially to channel conductance. As well, VCF studies of linked concatemers of KCNQ1 subunits support loose coupling between VSs and the gate (*38*), and when the pore is locked in the open state, VSs can still move between the resting and activated states (*58*). Last, our recent whole-cell and single-channel recordings have shown that the I_{Ks} (KCNQ1/KCNE1) channel complex can open and conduct current before all four VS domains have moved, with a minimum of one activatable VSD (*36*, *47*).

Models incorporating independent VS movement fit the data

Collectively, our results indicate that in the tetrameric KCNQ2 channel complex, only one VS is required to move to allow ion conduction at the whole-cell and single-channel levels, negating the requirement for a concerted transition of all four activated VSs to allow the channel to conduct. A model was built to reflect this experimental reality, with a resting state, four horizontally connected activatable VS states, and a single parallel lower tier of open states (Fig. 7A). Voltage-dependent kinetic constants for VS activation were derived from Q* oocyte fluorescence data (fig. S1) and for the opening transitions by optimizing model fits to current and fluorescence steady-state $G(V)$ and $F(V)$ relationships. The foot of the $F(V)$ relation is quite shallow, and good fits to this region using a single fluorescence component associated with horizontal transitions in the model gave a too-shallow relationship at the top of the curve compared with experimental data. We consistently found that including a second fluorescence component associated with the opening transition (a steeper F2, $k = 14.4$ mV in Fig. 7E) gave a much better fit to the overall $F(V)$ relationship for F192C-KCNQ2. The decreased slope of the Q* $F(V)$ relationship compared with the $G(V)$ relationship at P_o values less than 0.5 (Fig. 7, B and D) reflects the kinetics of the voltage-dependent opening step, which are subtly different from rate constants defining VS-activating transitions. Using these rate constants in the simpler models with only two or a single activatable VS simulates the overlap of oocyte $G(V)$ and $F(V)$ data from Q* and Q*Q_i (Fig. 2 and fig. S1) and reproduces the lack of significant $G(V)$ shifts between QQQQ, QQQ$_i$Q$_i$, and QQ$_i$Q$_i$Q$_i$ channels expressed in tsA201 cells (Fig. 4). The midpoints of current activation ($GV_{1/2}$) from channels bearing one, two, or three restricted VSDs all fall within the voltage range of the $GV_{1/2}$ of wt KCNQ2 channels (Fig. 4).

Allosteric regulation of the opening transition of activated KCNQ2 VS subunits is not required in any of the models to simulate the $G(V)$s, which supports the broad applicability of our models and sets it apart from other ion channels where positive allosteric modulation of subunit activation is required to accurately simulate channel gating (*37*, *42*, *47*). Analysis of the activation of the BK channel (*42*) showed that a higher open probability could be achieved with the activation of more VS domains, and better fits of model to experimental data were obtained with a positive allosteric model of activation gating rather than one incorporating a late concerted step. In KCNQ1 (*46*) and the I_{Ks} (KCNQ/KCNE1) channel complex (*47*), allosteric activation models are also required to accurately simulate the activation kinetics and steady-state current and fluorescence relationships with membrane voltage.

The lack of positive allosteric regulation in KCNQ2 opening [present in KCNQ1 (*36*)] may be explained from the distinctive structural arrangements of the VSD subunits and associated calmodulin (CaM) proteins between KCNQ2/CaM and KCNQ1/CaM complexes (fig. S9). As shown in the recent cryo-EM structures of KCNQ2 and KCNQ4 bound to CaM [KCNQ2/CaM (*59*) and KCNQ4/CaM (*60*)], there appears to be more space between VSD subunits in the C

terminus for the A-B helices and bound CaM than the narrow spaces between activating subunits found in the KCNQ1/CaM complex (fig. S9). This wider space in between VSD subunits of the KCNQ2 channel may facilitate the rest/active transitions of individual VS to open the channel without requiring cooperative engagement of subsequent VS activation, as suggested for KCNQ1/CaM channels (fig. S9, A to D).

Single-channel recordings reveal subunit-dependent conductance states

Single-channel recordings from tetrameric KCNQ2 channel assemblies containing variable numbers of activatable VSs revealed different subconductance states such that the larger the number of VSDs containing the E140R mutation, the smaller the unitary conductance, as fewer VSs are able to activate. Thus, channels containing three VSDs restrained in the resting state and only one activatable VSD subunit ($QQ_iQ_iQ_i$) have a smaller conductance and briefer openings than wt or channels bearing only one restrained VSD (Fig. 5). However, KCNQ2 channels bearing two activatable and two restrained VSDs exhibit different unitary conductance depending on the spatial configuration of the restricted VSDs. Concatemers containing two restrained VSDs (E140R) across from each other (QQ_iQQ_i) have a similar conductance to channels bearing three restrained VSDs ($QQ_iQ_iQ_i$; Fig. 6B). In contrast, concatemers containing E140R subunits next to each other (QQQ_iQ_i) exhibit a markedly larger conductance compared to both QQ_iQQ_i and $QQ_iQ_iQ_i$ constructs (Fig. 5).

To gain insight into how the placement of E140R subunits in the channel complex might affect conductance, we created homology structural models of KCNQ2 channels containing increasing numbers of VSDs in the resting state using the closed [PDB (Protein Data Bank): 8j05] and open (PDB: 8ijk) KCNQ2 channel structures (fig. S10) (*59*, *61*). When the KCNQ2 channel gate is closed (no K^+ permeation), the four opposing S314 residues in the S6 helices make up the narrowest part of the inner vestibule and prevent K^+ ions flowing through, as previously shown (fig. S10A) (*59*, *61*). Moving only one VS to its activated state causes the S6 to twist and move away from the inner pore, increasing the space between the S314 residues to allow some K^+ conduction (fig. S10C). Further activation of two, three, and all four VSs causes larger dilations of this entrance to the inner vestibule that facilitates the larger conductance of KCNQ2 channels. This structural model shows that KCNQ2 channels containing two restrained VSDs across from each other (fig. S10E) have smaller inner vestibule dimensions than those containing two restrained VSD subunits adjacent to each other (fig. S10F), which is consistent with the higher conductance observed for the QQQ_iQ_i construct than for QQ_iQQ_i in our single-channel results (Figs. 5 and 6 and fig. S10G). These differences contrast with what is observed in KCNQ1 + KCNE1 channels where two restrained VSDs, irrespective of their configuration within the tetramer, have a similar unitary conductance (*36*), presumably due to the slightly larger distances between S349 residues in the closed-state subunits compared to KCNQ2 and lower conductance of I_{Ks} (compare figs. S10 and S11).

Our findings suggest that various subconductance levels for KCNQ2 could arise from different numbers and arrangements of activated VSs, which then change the effective size of the open channel pore delimited by the four S314 residues. Together, these studies support an allosteric gating model in which gate opening can occur to small or intermediate subconductance levels "over a range of early and intermediate VS translations," which deviates from the canonical understanding of Kv channel gating. In the all-points histograms of the wt and E140R mutants, extra peaks are evident at smaller amplitudes that correspond to the main peaks of mutant channels (see arrows in Fig. 5B). Similar gating paradigms, whereby multiple subconductance state occupancy defines ion permeation characteristics, have been previously observed for drk1 (*62*, *63*) and Kir2.2 (*64*) K^+ channels and Na^+-activated K^+ channels (*65*) [of weak voltage sensitivity; (*66*)] and in glutamate receptors (*67*). However, a gating scheme involving regulation of subconductance levels by the number and arrangement of activated VSs, which then determine the open pore dimensions shown here for KCNQ2, has not been previously demonstrated in other voltage-gated (Kv) K^+ channel family members and may represent either an exception here in the highly homologous KCNQ channel subfamily or a (yet unconfirmed) mechanism shared by Kv channels in general.

Implications of single subunit activation for the pathophysiology of multimeric channels

All five members of the KCNQ channel family are activated by membrane depolarization and phosphatidylinositol 4,5-bisphosphate and regulated by CaM and phosphorylation (*68*–*72*). Despite these shared properties and high structural homology, only the neuronal subfamily members KCNQ2 to KCNQ5 have been shown to associate in different combinations to form functional heteromeric voltage-gated K^+ (M-type) channels in different neuronal areas, which allows functional versatility in different brain regions (*13*, *14*, *73*). Here, we show that a single activated subunit opens KCNQ2 channels and that recruitment of additional VSs does not additionally favor opening energetics (Figs. 4 and 7). If this is also the case for various combinations of subunits in heteromeric KCNQx channels, then the $V_{1/2}$ of the resulting $G(V)$ curve may be substantially affected by subunits from the channel type with the most hyperpolarized activation, as these would open "first" during depolarization and contribute notably to the overall channel conductance (Fig. 8). This feature might be important during development, as KCNQ2 expression appears earlier than KCNQ3 and possibly KCNQ5 (*16*, *17*) channels.

Our work also provides a framework for understanding the variation in the severity of neuronal KCNQ channelopathies caused by GOF and LOF gating mutations. If KCNQ3 and KCNQ5 can also open upon activation of a single VS, like KCNQ2, then in heteromeric KCNQ2/3, KCNQ2/5, or KCNQ3/5 channels, the voltage dependence of opening will be determined by subunits with the most hyperpolarized $V_{1/2}$. For heterozygous mutations, if wt and mutant subunits assemble randomly, it has been predicted that 94% of the assembled channels will contain one or more mutant subunits (*74*–*76*). In the case of a LOF gating mutation in one of the alleles, since the $V_{1/2}$ of wt subunits is hyperpolarized compared with LOF mutant subunits, the $G(V)$ curve would be predominantly determined by the 94% of channels with one or more wt subunits (Fig. 8, blue diamonds). The 6% of channels with four mutant subunits would have a depolarized $V_{1/2}$, which will extend saturation of the maximum conductance to more positive voltages, but have a limited effect on the currents within the physiological range (Fig. 8, blue triangles). Therefore, heterozygous channels bearing LOF mutations will likely display mild phenotypes, as

only 6% of the channels will have substantially depolarized half-activation voltages.

Conversely, for heterozygous GOF gating mutations, where the $V_{1/2}$ of the mutant subunits is more negative than wt subunits, 94% of the assembled channels would exhibit a pathological component of $G(V)$ at negative voltages (compare Fig. 8E and fig. S8, green squares) and likely a hyperpolarized $V_{1/2}$ as well. Since extra currents around the resting potential and in the early activation range of potentials are highly likely to be excitotoxic, our results suggest that GOF heterozygous mutations in which a single active subunit is sufficient to open the channel will exhibit a more severe phenotype than LOF mutations.

In conclusion, our study reveals that KCNQ2 channels do not require a concerted movement of all four subunits but rather that channel opening can occur with activation of a single VS. Subsequent recruitment of additional VSs does not facilitate channel opening, indicating the absence of positive allosterism in opening. This gating behavior has important implications for the current-voltage phenotypes of GOF and LOF mutations. Single-channel analysis of tetrameric channel assemblies containing variable numbers of activatable VSs reveals different subconductance states such that the smaller the number of VSs restrained in the resting state, the larger the unitary conductance of KCNQ2 channels. This gradual increase in conductance is not favored by incremental activation of additional VSs within the tetramer, but it is determined by the progressive dilation of the activation gate.

MATERIALS AND METHODS

Chemicals

MTSET was purchased from Toronto Research Chemicals Inc. (Downsview, ON, Canada). Alexa Fluor 488 C5 maleimide was purchased from Thermo Fisher Scientific (Waltham, MA). All other chemicals were obtained from Sigma-Aldrich (St. Louis, MO).

Molecular biology

The full-length human KCNQ2 constructs (NCBI Reference Sequence: NP_742105.1; GenInfo Identifier: 26051264) and tandem dimers and tetramers of KCNQ2 (linkers in between subunits were composed of 25 glycine residues) were synthesized (GenScript USA, Piscataway, NJ) and ligated between the Bam HI and Xba I sites in the multiple cloning site into the pGEM-HE vector for oocyte expression or the pcDNA3.1 for mammalian cell expression. The pGEM vector had been previously modified to contain a T7 promoter and 3′ and 5′ untranslated regions from the *Xenopus* β-*globin* gene (*77*). The Kozak consensus sequence (GCCACC) and the Bg III (AGATCT) or (Age I) (ACCGGT) restriction sites were added before the start codon (ATG) of the *KCNQ2* gene. Point mutations were made in the *KCNQ2* gene using the Quikchange XL site-directed Mutagenesis kit (Agilent) according to the manufacturer's protocol. The correct incorporation of the specific variant was assessed by Sanger sequencing (sequencing by Genewiz LLC, South Plainfield, NJ). For oocyte experiments, the RNAs were synthesized in vitro using the mMessage mMachine T7 RNA Transcription Kit (Thermo Fisher Scientific) from the linearized cDNA. mRNA (40 to 50 nl) was injected into *Xenopus laevis* oocytes (purchased from Ecocyte) using a Nanoject II nanoinjector (Drummond Scientific), and electrophysiological experiments were performed 2 to 5 days after injection.

Cell surface biotinylation and Western blots

Oocytes were injected with 41.4 nl of mRNA (2 to 3 μg/μl) from wt KCNQ2 or the KCNQ2-E140R mutation. Following incubation in an ND96 solution for 72 hours at 18°C, the oocytes were washed twice with phosphate-buffered saline with Ca/Mg (PBS-CM) (in 137 mM NaCl, 2.7 mM KCl, 10 mM Na_2HPO_4, 1.8 mM KH_2PO_4, 0.1 mM $CaCl_2$, and 1 mM $MgCl_2$), and surface proteins from 40 oocytes per construct were labeled using EZ-Link Sulfo-NHS-SS-Biotin (Thermo Fisher Scientific) and dissolved to a final concentration of 1.25 mg ml^{-1} in ice-cold PBS-CM. Following agitation for 30 min, the reaction was quenched for 30 min using quenching buffer (PBS-CM supplemented with 200 mM glycine). Next, the oocytes were lysed using lysis buffer (150 mM NaCl, 100 mM tris-HCl, 0.1% SDS, and 1% Triton X-100) with added Halt protease inhibitor cocktail (1:100) (Thermo Fisher Scientific). Biotin-labeled surface proteins were isolated and purified using Pierce Spin Columns-Snap Cap (Thermo Fisher Scientific) with 500 μl of Pierce NeutrAvidin Agarose added to each column (Thermo Fisher Scientific). The total protein was quantified using Pierce BCA protein assay kit (23225, Thermo Fisher Scientific). Purified surface proteins or total cell lysates were separated on a 4 to 15% TGX precast gel (Bio-Rad) at 120 V for 2 hours and transferred to a 0.2-μm polyvinylidene difluoride membrane (Bio-Rad), with a 7-min transfer time (25 V and 2.5 A, Trans-Blot Turbo system). Membranes were incubated in LI-COR blocking buffer for 1 hour, followed by incubation in LI-COR blocking buffer containing either rabbit polyclonal anti-KCNQ2 (PA1-929; Invitrogen, 1:1000), mouse polyclonal anti-β-actin (A5441; Sigma-Aldrich, 1:2000), and mouse anti-Na^+/K^+ ATPase (adenosine triphosphatase; 05-369; EMD Merck Millipore, 1:1000) at 4°C overnight. Next, the membranes were washed 5 times for 5 min with TBST (20 mM tris-HCl, 150 mM NaCl, and 0.1% Tween 20, pH 7.5) and incubated with secondary antibodies [horseradish peroxidase–conjugated goat anti-rabbit immunoglobulin G (H + L) (1:5000, 111-035-144; Jackson ImmunoResearch Laboratories) and goat anti-mouse immunoglobulin G (1:5000, G21040; Invitrogen)] in LI-COR blocking buffer for 1 hour at room temperature in the dark. Last, the membranes were washed 5 times for 5 min in TBST. Antibody-bound peroxidase was detected by enhanced chemiluminescence (Clarity Western ECL Substrate, Bio-Rad), and the chemiluminescent signals were captured using a ChemiDoc imaging system (Bio-Rad).

TEVC recordings

TEVC recordings were performed as previously described (*77*). A regular ND96 solution for TEVC contained 96 mM NaCl, 2 mM KCl, 1 mM $MgCl_2$, 1.8 mM $CaCl_2$, and 5 mM Hepes (pH = 7.5). Ionic currents were recorded in TEVC using an OC-725C oocyte clamp (Warner Instruments), low-pass filtered at 1 kHz, and sampled at 5 kHz. Microelectrodes were pulled using borosilicate glass to resistances from 0.3 to 0.5 megohms when filled with 3 M KCl. Voltage clamp data were digitized at 5 kHz (Axon Digidata 1440A; Molecular Devices), collected using pClamp 10 (Axon Instruments). Note that while ordinarily oocyte data using monomeric (single) constructs would better reflect the decrease in amplitudes, this is not the case with the tetrameric constructs because the synthesis of the long RNA molecules is not very efficient, and it is difficult to know how much of the complete sequence is actually being injected into each oocyte.

Cysteine accessibility measurements in TEVC recordings

We performed cysteine accessibility to the MTS reagent MTSET in TEVC recordings following procedures previously described in (*21*). Briefly, an ND96 solution for TEVC containing 96 mM NaCl, 2 mM KCl, 1 mM $MgCl_2$, 1.8 mM $CaCl_2$, and 5 mM Hepes (pH = 7.5) was perfused using a computer-driven, valve-controlled, home-made perfusion system that allowed for a rapid switching (within 2 s) between ND96 and MTS reagents during either the open or closed protocol. We adapted the open- and closed-state protocols (*23*) to study the solvent exposure of the substituted cysteines (Cys) in S3-S4 and S4 and test whether these Cys residues were exposed in open and/or closed channels using irreversible covalent modification by MTSET. Briefly, cells were held at −80 mV for 1 s before stepping to +20 mV for 12 s and then repolarized for another 12 s to −80 mV (for the open state) or voltages between −80 and −140 mV (for the closed state) before stepping to the test potential (+20 mV) to measure the change in currents induced by several 5-s cycles of MTS reagents (see black rectangles in protocols on the top) (*21*). We repeat 5-s MTSET application in between 25-s washouts for 8 to 12 cycles, as shown in the open and closed protocols at the top of Fig. 3, following similar procedures described in (*21*). The MTSET concentration was 100 μM. Ionic currents were recorded in TEVC as described above. Results are presented as means ± SEM (*n*, number of measurements).

Voltage clamp fluorometry

VCF experiments were carried out as previously reported (*21*). Briefly, aliquots of 50 ng of mRNA coding for the cysteine mutant KCNQ2-F192C were injected into *X. laevis* oocytes. At 2 to 5 days after injection, oocytes were labeled for 30 min with 100 μM Alexa Fluor 488 maleimide (Thermo Fisher Scientific) in high-[K^+] solution (98 mM KCl, 1.8 mM $CaCl_2$, 1 mM $MgCl_2$, and 5 mM Hepes, pH 7.05) at 4°C in the dark. The labeled oocytes were then rinsed three to five times in dye-free ND96 and kept on ice before each recording to prevent internalization of labeled channels. Oocytes were placed into a recording chamber animal pole "up" in an ND96 solution (pH 7.5 with NaOH), and electrical measurements were carried out in TEVC using an Axoclamp 900A amplifier (Molecular Devices). Microelectrodes were pulled to resistances from 0.3 to 0.5 megohms when filled with 3 M KCl. Voltage clamp data were digitized at 5 kHz (Axon Digidata 1550B via a digital Axoclamp 900A commander, Molecular Devices) and collected using pClamp 10 (Axon Instruments). Fluorescence recordings were performed using an Olympus BX51WI upright microscope. Light was focused on the top of the oocyte through a 20× water immersion objective [numerical aperture (NA), 1.0; working distance, 2 mm] after being passed through an Oregon green filter cube (41026; Chroma). Fluorescence signals were focused on a photodiode and amplified with an Axopatch 200B patch clamp amplifier (Axon Instruments). Fluorescence signals were low-pass Bessel filtered (Frequency Devices) at 100 to 200 Hz, digitized at 1 kHz, and recorded using pClamp 10. When needed, we added 100 μM $LaCl_3$ to the batch solution to block endogenous hyperpolarization-activated currents. At this concentration, La^{3+} did not affect $G(V)$ or $F(V)$ curves from KCNQ2 channels.

Patch clamp electrophysiology

tsA201 and HEKt (human embryonic kidney 293t cell line) cells plated on coverslips were transfected 24 hours later using Lipofectamine2000 (Thermo Fisher Scientific) as per the manufacturer's protocol. The channel constructs were transfected with green fluorescent protein (GFP) in a 3:1 ratio. All experiments were performed 24 to 48 hours posttransfection at room temperature. Successfully transfected cells were identified by GFP fluorescence.

Whole-cell voltage clamp recordings in HEKt cells were made using an inverted Nikon microscope (Eclipse TE2000-U) custom made for fluorescence and equipped with a 20× 0.8-NA and 40× 0.8-NA objectives. Cells were continuously perfused with a bath solution (140 mM NaCl, 2.4 mM KCl, 1.3 mM $MgCl_2$, 2.5 mM $CaCl_2$, 10 mM Hepes, and 10 mM D-glucose, pH 7.4). Records were made at room temperature (~22°C). Patch pipettes were pulled from borosilicate glass (outer diameter, 1.5 mm; inner diameter, 0.86 mm; Sutter Instruments) using a horizontal puller (P-97 Sutter Instruments) and had a resistance of 2 to 5 megohms when filled with the intracellular solution (125 mM K-gluconate, 10 mM NaCl, 1 mM EGTA, 4 mM Na_2-ATP, 10 mM Hepes, and 10 mM D-glucose, pH 7.4). Voltage clamp and current clamp recordings were acquired using an Axopatch 200B amplifier (Molecular Devices, US), digitized at 10 kHz (filtered at 5 kHz, Axon Digidata 1550; Molecular Devices), and collected using pClamp 11 (Axon Instruments). Cells were held at −80 mV followed by a step from −100 to +60 mV (in 10- or 20-mV steps) for 2 s, followed by a subsequent voltage step to −50 mV before returning to the −80-mV holding potential.

Whole-cell currents in tsA201 were acquired using an Axopatch 200B amplifier, Digidata 1440A, and pClamp 10 software (Molecular Devices, San Jose, CA). Electrode pipettes were pulled on a linear multistage electrode puller (Sutter Instrument, Novato, CA) from thin-walled borosilicate glass (World Precision Instruments, Sarasota, FL) and fire polished before use. Electrode resistances were between 1 and 2 megohms, with series resistances <4 megohms. A series resistance compensation of ~80% was applied to all whole-cell recordings, with a calculated voltage error of ~1 mV/nA current. Sampling was at 10 kHz and filtered at 2 to 5 kHz (*78*). The bath solution contained 135 mM NaCl, 5 mM KCl, 1 mM $MgCl_2$, 2.8 mM Na-acetate, and 10 mM Hepes (pH 7.4 with NaOH); and the pipette solution contained 130 mM KCl, 5 mM EGTA, 1 mM $MgCl_2$, 4 mM Na_2-ATP, 0.1 mM guanosine 5′-triphosphate, and 10 mM Hepes (pH 7.2 with KOH).

Single-channel recording

Cell-attached recordings were made from mouse *ltk*− fibroblasts (American Type Culture Collection catalog no. CCL-1.3; Cedarlane Labs, Burlington, Ontario, Canada) plated on glass coverslips and transfected 24 hours later using Lipofectamine 2000 (Thermo Fisher Scientific). Cells were transfected with 1.5 μg of channel DNA and 0.75 μg of GFP:pcDNA3 as a marker for transfected cells. Recordings were acquired using an Axopatch 200B amplifier, Digidata 1440A, and pClamp 10 software (Molecular Devices, San Jose, CA). Pipettes were made from thick-walled borosilicate glass (Sutter Instruments, Novato, CA) using a linear multistage electrode puller (Sutter Instruments). Resistances of the electrodes after fire polishing were between 30 and 80 megohms. Sylgard (Dow Corning, Midland, MI) was applied to electrodes before use. Sampling was at 10 kHz, with low-pass filtering of 2 kHz at acquisition using a −3-dB, four-pole Bessel filter. Records were then digitally filtered at 200 Hz for presentation and analysis (*71*, *78*, *79*). Solutions were as follows: The bath solution contained 135 mM KCl, 1 mM $MgCl_2$, 1 mM $CaCl_2$, 10 mM Hepes, and 10 mM dextrose (pH 7.4 with KOH). The pipette solution contained 6 mM NaCl, 129 mM MES, 1 mM $MgCl_2$, 5 mM KCl, 1 mM $CaCl_2$, and 10 mM Hepes (pH 7.4 with NaOH).

Amplitudes of channel openings were determined from Gaussian fits of all-points histograms in Clampfit 10 (Molecular Devices). Conductance curves were plotted using Prism10 (GraphPad Software, San Diego, CA).

Modeling

MATLAB R2023b (MathWorks, Natick, MA; RRID:SCR_001622) was used to write scripts to simulate KCNQ2 activation and fluorescence from the F192C-labeled mutant channel (fig. S1) and from channels with up to three of the four subunits containing the S4 mutation E140R (e.g., Fig. 4). The MATLAB subroutines "ode23s" and "fminsearchbnd" with boundaries (*80*), respectively, were used to solve differential equations using a Jacobian matrix and optimize rate constants and model fits to steady-state $G(V)$, $F(V)$, and tau(V) relationships using a bounded Nelder Mead optimization algorithm (*81*, *82*). Transition rates were optimized by minimizing through iteration a scalar function that simultaneously evaluated the squared errors (SumSq) between computed and experimental data values (*47*). Where possible, boundaries limited parameter values to being close to experimental values. Model schemes are shown in Fig. 7A, and the subscript R or A indicates the number of resting or activated subunits, respectively. Closed and open channel states are indicated as "C" and "O," respectively. Forward and backward rate constants in model schemes are indicated as "α" and "β" for the horizontal VS transitions, while voltage-dependent transition rates related to any second VS movement and pore coupling in the opening step are denoted by "δ" and "γ" for opening and closing rates, respectively. To obtain α, β, δ, and γ rate constants, rate versus voltage plots were fit with Eq. 1

$$\text{Rate constant (V)} = \text{rate constant (0 mV)} \times e^{\frac{zVF}{RT}} \quad (1)$$

where V and 0 refers to voltage in mV; z is the apparent valence; and F, R, and T have their usual meanings. At room temperature (22°C), $F/RT = 0.39$. After optimization, rate constants and z values used in the model for plots in Fig. 7 were as follows: $\alpha_0 = 0.0161\ \text{ms}^{-1}$, $z_\alpha = 0.551$; $\beta_0 = 9.41 \times 10^{-4}\ \text{ms}^{-1}$, $z_\beta = -0.365$; $\delta_0 = 8.92 \times 10^{-3}\ \text{ms}^{-1}$, $z_\delta = 0.977$; $\gamma_0 = 3.04 \times 10^{-5}\ \text{ms}^{-1}$, $z_\gamma = -0.895$.

Electrophysiology data analysis

Data were analyzed with Clampfit 10 (Axon Instruments, Inc., Sunnyvale, CA), OriginPro 2021b (OriginLabs Northampton, MA), and Corel-DRAW Graphics Suite 2021 software. To determine the ionic conductance established by a given test voltage, a test voltage pulse was followed by a step to the fixed voltage of −40 mV (tail), and the current was recorded following the step. To estimate the conductance $g(V)$ activated at the end of the test pulse to voltage V, the current flowing after the hook was exponentially extrapolated to the time of the step and divided by the offset between −40 mV and the reversal potential. The conductance $g(V)$ associated with different test voltages V in a given experiment was fitted by the relation

$$g(V) = A_1 + \left(A_2 - A_1\right) / \left\{1 + \exp\left[\left(V_{1/2} - V\right)/\kappa\right]\right\} \quad (2)$$

where A_1 and A_2 are conductances that would be approached at extreme negative or positive voltages, respectively; $V_{1/2}$ is the voltage that activates the conductance $\left(A_1 + A_2\right)/2$; and κ is the slope factor in millivolts. Because of the generally different numbers of expressed channels in different oocytes, we compare normalized conductance, $G(V)$

$$G(V) = g(V)/A_2 \quad (3)$$

Fluorescence signals were corrected for bleaching and time averaged over 10- to 40-ms intervals for analysis. The voltage dependence of fluorescence $f(V)$ was analyzed and normalized $[F(V)]$ using relations analogous to those for conductance (Eqs. 2 and 3).

Statistics

All experiments were repeated three or more times from at least three batches of oocytes and cells. Pairwise comparisons were achieved using an analysis of variance (ANOVA) and Bonferroni's post hoc test or Student's t test, as indicated in each figure. Data are represented as means ± SEM, and "n" represents the number of experiments.

Supplementary Materials

This PDF file includes:
Figs. S1 to S11

REFERENCES AND NOTES

1. T. Jespersen, M. Grunnet, S. P. Olesen, The KCNQ1 potassium channel: From gene to physiological function. *Phys. Ther.* **20**, 408–416 (2005).
2. T. J. Jentsch, Neuronal KCNQ potassium channels: Physiology and role in disease. *Nat. Rev. Neurosci.* **1**, 21–30 (2000).
3. D. A. Brown, P. R. Adams, Muscarinic suppression of a novel voltage-sensitive K^+ current in a vertebrate neurone. *Nature* **283**, 673–676 (1980).
4. J. V. Halliwell, P. R. Adams, Voltage-clamp analysis of muscarinic excitation in hippocampal neurons. *Brain Res.* **250**, 71–92 (1982).
5. B. Hille, *Ion Channels of Excitable Membranes* (Sinauer Associates Inc., ed. 3, 2001).
6. S. Maljevic, H. Lerche, Potassium channel genes and benign familial neonatal epilepsy. *Prog. Brain Res.* **213**, 17–53 (2014).
7. T. T. Sands, F. Miceli, G. Lesca, A. E. Beck, L. G. Sadleir, D. K. Arrington, B. Schonewolf-Greulich, S. Moutton, A. Lauritano, P. Nappi, M. V. Soldovieri, I. E. Scheffer, H. C. Mefford, N. Stong, E. L. Heinzen, D. B. Goldstein, A. G. Perez, E. H. Kossoff, A. Stocco, J. A. Sullivan, V. Shashi, B. Gerard, C. Francannet, A. M. Bisgaard, Z. Tumer, M. Willems, F. Rivier, A. Vitobello, K. Thakkar, D. S. Rajan, A. J. Barkovich, S. Weckhuysen, E. C. Cooper, M. Taglialatela, M. R. Cilio, Autism and developmental disability caused by *KCNQ3* gain-of-function variants. *Ann. Neurol.* **86**, 181–192 (2019).
8. T. Wang, K. Hoekzema, D. Vecchio, H. Wu, A. Sulovari, B. P. Coe, M. A. Gillentine, A. B. Wilfert, L. A. Perez-Jurado, M. Kvarnung, Y. Sleyp, R. K. Earl, J. A. Rosenfeld, M. R. Geisheker, L. Han, B. Du, C. Barnett, E. Thompson, M. Shaw, R. Carroll, K. Friend, R. Catford, E. E. Palmer, X. Zou, J. Ou, H. Li, H. Guo, J. Gerdts, E. Avola, G. Calabrese, M. Elia, D. Greco, A. Lindstrand, A. Nordgren, B. M. Anderlid, G. Vandeweyer, A. Van Dijck, N. Van der Aa, B. McKenna, M. Hancarova, S. Bendova, M. Havlovicova, G. Malerba, B. D. Bernardina, P. Muglia, A. van Haeringen, M. J. V. Hoffer, B. Franke, G. Cappuccio, M. Delatycki, P. J. Lockhart, M. A. Manning, P. Liu, I. E. Scheffer, N. Brunetti-Pierri, N. Rommelse, D. G. Amaral, G. W. E. Santen, E. Trabetti, Z. Sedlacek, J. J. Michaelson, K. Pierce, E. Courchesne, R. F. Kooy, S. Consortium, M. Nordenskjold, C. Romano, H. Peeters, R. A. Bernier, J. Gecz, K. Xia, E. E. Eichler, Large-scale targeted sequencing identifies risk genes for neurodevelopmental disorders. *Nat. Commun.* **11**, 4932 (2020).
9. K. Arredondo, C. Myers, E. Hansen-Kiss, M. T. Mathew, V. Jayaraman, A. Siemon, D. Bartholomew, G. E. Herman, M. Mori, Phenotypic spectrum in a family sharing a heterozygous *KCNQ3* variant. *J. Child Neurol.* **37**, 517–523 (2022).
10. M. V. Soldovieri, N. Boutry-Kryza, M. Milh, D. Doummar, B. Heron, E. Bourel, P. Ambrosino, F. Miceli, M. De Maria, N. Dorison, S. Auvin, B. Echenne, J. Oertel, A. Riquet, L. Lambert, M. Gerard, A. Roubergue, A. Calender, C. Mignot, M. Taglialatela, G. Lesca, Novel *KCNQ2* and *KCNQ3* mutations in a large cohort of families with benign neonatal epilepsy: First evidence for an altered channel regulation by syntaxin-1A. *Hum. Mutat.* **35**, 356–367 (2014).
11. C. Bellocq, A. C. van Ginneken, C. R. Bezzina, M. Alders, D. Escande, M. M. Mannens, I. Baro, A. A. Wilde, Mutation in the *KCNQ1* gene leading to the short QT-interval syndrome. *Circulation* **109**, 2394–2397 (2004).

12. X. Du, H. Gao, D. Jaffe, H. Zhang, N. Gamper, M-type K^+ channels in peripheral nociceptive pathways. *Br. J. Pharmacol.* **175**, 2158–2172 (2018).
13. H. S. Wang, Z. Pan, W. Shi, B. S. Brown, R. S. Wymore, I. S. Cohen, J. E. Dixon, D. McKinnon, KCNQ2 and KCNQ3 potassium channel subunits: Molecular correlates of the M-channel. *Science* **282**, 1890–1893 (1998).
14. B. C. Schroeder, M. Hechenberger, F. Weinreich, C. Kubisch, T. J. Jentsch, KCNQ5, a novel potassium channel broadly expressed in brain, mediates M- type currents. *J. Biol. Chem.* **275**, 24089–24095 (2000).
15. H. Soh, R. Pant, J. J. LoTurco, A. V. Tzingounis, Conditional deletions of epilepsy-associated KCNQ2 and KCNQ3 channels from cerebral cortex cause differential effects on neuronal excitability. *J. Neurosci.* **34**, 5311–5321 (2014).
16. T. Kanaumi, S. Takashima, H. Iwasaki, M. Itoh, A. Mitsudome, S. Hirose, Developmental changes in KCNQ2 and KCNQ3 expression in human brain: Possible contribution to the age-dependent etiology of benign familial neonatal convulsions. *Brain Dev.* **30**, 362–369 (2008).
17. C. Gomis-Perez, J. Urrutia, A. Marce-Grau, C. Malo, E. Lopez-Laso, A. Felipe-Rucian, M. Raspall-Chaure, A. Macaya, A. Villarroel, Homomeric Kv7.2 current suppression is a common feature in *KCNQ2* epileptic encephalopathy. *Epilepsia* **60**, 139–148 (2019).
18. X. Li, Q. Zhang, P. Guo, J. Fu, L. Mei, D. Lv, J. Wang, D. Lai, S. Ye, H. Yang, J. Guo, Molecular basis for ligand activation of the human KCNQ2 channel. *Cell Res.* **31**, 52–61 (2021).
19. S. B. Long, E. B. Campbell, R. Mackinnon, Crystal structure of a mammalian voltage-dependent *Shaker* family K^+ channel. *Science* **309**, 897–903 (2005).
20. D. del Camino, G. Yellen, Tight steric closure at the intracellular activation gate of a voltage- gated K^+ channel. *Neuron* **32**, 649–656 (2001).
21. M. A. Edmond, A. Hinojo-Perez, X. Wu, M. E. Perez Rodriguez, R. Barro-Soria, Distinctive mechanisms of epilepsy-causing mutants discovered by measuring S4 movement in KCNQ2 channels. *eLife* **11**, e77030 (2022).
22. L. M. Mannuzzu, M. M. Moronne, E. Y. Isacoff, Direct physical measure of conformational rearrangement underlying potassium channel gating. *Science* **271**, 213–216 (1996).
23. H. P. Larsson, O. S. Baker, D. S. Dhillon, E. Y. Isacoff, Transmembrane movement of the *Shaker* K^+ channel S4. *Neuron* **16**, 387–397 (1996).
24. S. A. Seoh, D. Sigg, D. M. Papazian, F. Bezanilla, Voltage-sensing residues in the S2 and S4 segments of the *Shaker* K^+ channel. *Neuron* **16**, 1159–1167 (1996).
25. S. K. Aggarwal, R. MacKinnon, Contribution of the S4 segment to gating charge in the *Shaker* K^+ channel. *Neuron* **16**, 1169–1177 (1996).
26. F. Bezanilla, E. Perozo, The voltage sensor and the gate in ion channels. *Adv. Protein Chem.* **63**, 211–241 (2003).
27. A. L. Hodgkin, A. F. Huxley, A quantitive description of membrane current and its application to conduction and excitation in nerve. *J. Physiol.* **117**, 500–544 (1952).
28. W. N. Zagotta, T. Hoshi, J. Dittman, R. W. Aldrich, Shaker potassium channel gating. II: Transitions in the activation pathway. *J. Gen. Physiol.* **103**, 279–319 (1994).
29. N. E. Schoppa, F. J. Sigworth, Activation of *Shaker* potassium channels: III. An activation gating model for wild-type and V2 mutant channels. *J. Gen. Physiol.* **111**, 313–342 (1998).
30. F. J. Sigworth, Voltage gating of ion channels. *Q. Rev. Biophys.* **27**, 1–40 (1994).
31. J. L. Ledwell, R. W. Aldrich, Mutations in the S4 region isolate the final voltage-dependent cooperative step in potassium channel activation. *J. Gen. Physiol.* **113**, 389–414 (1999).
32. S. B. Long, E. B. Campbell, R. Mackinnon, Voltage sensor of Kv1.2: Structural basis of electromechanical coupling. *Science* **309**, 903–908 (2005).
33. S. B. Long, X. Tao, E. B. Campbell, R. MacKinnon, Atomic structure of a voltage-dependent K^+ channel in a lipid membrane-like environment. *Nature* **450**, 376–382 (2007).
34. B. Roux, Dissecting the coupling between the voltage sensor and pore domains. *Neuron* **52**, 568–569 (2006).
35. A. I. Fernandez-Marino, T. J. Harpole, K. Oelstrom, L. Delemotte, B. Chanda, Gating interaction maps reveal a noncanonical electromechanical coupling mode in the Shaker K^+ channel. *Nat. Struct. Mol. Biol.* **25**, 320–326 (2018).
36. M. Westhoff, J. Eldstrom, C. I. Murray, E. Thompson, D. Fedida, IKs ion-channel pore conductance can result from individual voltage sensor movements. *Proc. Natl. Acad. Sci. U.S.A.* **116**, 7879–7888 (2019).
37. C. Altomare, A. Bucchi, E. Camatini, M. Baruscotti, C. Viscomi, A. Moroni, D. DiFrancesco, Integrated allosteric model of voltage gating of HCN channels. *J. Gen. Physiol.* **117**, 519–532 (2001).
38. J. D. Osteen, R. Barro-Soria, S. Robey, K. J. Sampson, R. S. Kass, H. P. Larsson, Allosteric gating mechanism underlies the flexible gating of KCNQ1 potassium channels. *Proc. Natl. Acad. Sci. U.S.A.* **109**, 7103–7108 (2012).
39. M. A. Zaydman, M. A. Kasimova, K. McFarland, Z. Beller, P. Hou, H. E. Kinser, H. Liang, G. Zhang, J. Shi, M. Tarek, J. Cui, Domain-domain interactions determine the gating, permeation, pharmacology, and subunit modulation of the IKs ion channel. *eLife* **3**, e03606 (2014).
40. B. S. Rothberg, K. L. Magleby, Kinetic structure of large-conductance Ca^{2+}-activated K^+ channels suggests that the gating includes transitions through intermediate or secondary states. A mechanism for flickers. *J. Gen. Physiol.* **111**, 751–780 (1998).
41. D. H. Cox, J. Cui, R. W. Aldrich, Allosteric gating of a large conductance Ca-activated K^+ channel. *J. Gen. Physiol.* **110**, 257–281 (1997).
42. F. T. Horrigan, J. Cui, R. W. Aldrich, Allosteric voltage gating of potassium channels I. Mslo ionic currents in the absence of Ca^{2+}. *J. Gen. Physiol.* **114**, 277–304 (1999).
43. L. J. Ma, I. Ohmert, V. Vardanyan, Allosteric features of KCNQ1 gating revealed by alanine scanning mutagenesis. *Biophys. J.* **100**, 885–894 (2011).
44. F. T. Horrigan, R. W. Aldrich, Coupling between voltage sensor activation, Ca2+ binding and channel opening in large conductance (BK) potassium channels. *J. Gen. Physiol.* **120**, 267–305 (2002).
45. J. Yang, G. Krishnamoorthy, A. Saxena, G. Zhang, J. Shi, H. Yang, K. Delaloye, D. Sept, J. Cui, An epilepsy/dyskinesia-associated mutation enhances BK channel activation by potentiating $Ca2^+$ sensing. *Neuron* **66**, 871–883 (2010).
46. J. D. Osteen, C. Gonzalez, K. J. Sampson, V. Iyer, S. Rebolledo, H. P. Larsson, R. S. Kass, KCNE1 alters the voltage sensor movements necessary to open the KCNQ1 channel gate. *Proc. Natl. Acad. Sci. U.S.A.* **107**, 22710–22715 (2010).
47. D. Fedida, D. Sastre, Y. Dou, M. Westhoff, J. Eldstrom, Evaluating sequential and allosteric activation models in IKs channels with mutated voltage sensors. *J. Gen. Physiol.* **156**, e202313465 (2024).
48. M. V. Soldovieri, P. Ambrosino, I. Mosca, F. Miceli, C. Franco, L. M. T. Canzoniero, B. Kline-Fath, E. C. Cooper, C. Venkatesan, M. Taglialatela, Epileptic encephalopathy in a patient with a novel variant in the Kv7.2 S2 transmembrane segment: Clinical, genetic, and functional features. *Int. J. Mol. Sci.* **20**, 3382 (2019).
49. R. Kanyo, S. M. Lamothe, A. Urrutia, S. J. Goodchild, W. T. Allison, R. Dean, H. T. Kurata, Site and mechanism of ML252 inhibition of Kv7 voltage-gated potassium channels. *Function* **4**, zqad021 (2023).
50. Y. Li, N. Gamper, M. S. Shapiro, Single-channel analysis of KCNQ K^+ channels reveals the mechanism of augmentation by a cysteine-modifying reagent. *J. Neurosci.* **24**, 5079–5090 (2004).
51. A. A. Selyanko, J. K. Hadley, D. A. Brown, Properties of single M-type KCNQ2/KCNQ3 potassium channels expressed in mammalian cells. *J. Physiol.* **534**, 15–24 (2001).
52. R. Barro-Soria, S. Rebolledo, S. I. Liin, M. E. Perez, K. J. Sampson, R. S. Kass, H. P. Larsson, KCNE1 divides the voltage sensor movement in KCNQ1/KCNE1 channels into two steps. *Nat. Commun.* **5**, 3750 (2014).
53. S. Weckhuysen, V. Ivanovic, R. Hendrickx, R. Van Coster, H. Hjalgrim, R. S. Moller, S. Gronborg, A. S. Schoonjans, B. Ceulemans, S. B. Heavin, C. Eltze, R. Horvath, G. Casara, T. Pisano, L. Giordano, K. Rostasy, E. Haberlandt, B. Albrecht, A. Bevot, I. Benkel, S. Syrbe, B. Sheidley, R. Guerrini, A. Poduri, J. R. Lemke, S. Mandelstam, I. Scheffer, M. Angriman, P. Striano, C. Marini, A. Suls, P. De Jonghe, KCNQ2 Study Group, Extending the KCNQ2 encephalopathy spectrum: Clinical and neuroimaging findings in 17 patients. *Neurology* **81**, 1697–1703 (2013).
54. F. Miceli, M. V. Soldovieri, P. Ambrosino, M. De Maria, M. Migliore, R. Migliore, M. Taglialatela, Early-onset epileptic encephalopathy caused by gain-of-function mutations in the voltage sensor of Kv7.2 and Kv7.3 potassium channel subunits. *J. Neurosci.* **35**, 3782–3793 (2015).
55. P. Castaldo, E. M. del Giudice, G. Coppola, A. Pascotto, L. Annunziato, M. Taglialatela, Benign familial neonatal convulsions caused by altered gating of KCNQ2/KCNQ3 potassium channels. *J. Neurosci.* **22**, RC199 (2002).
56. J. J. Millichap, F. Miceli, M. De Maria, C. Keator, N. Joshi, B. Tran, M. V. Soldovieri, P. Ambrosino, V. Shashi, M. A. Mikati, E. C. Cooper, M. Taglialatela, Infantile spasms and encephalopathy without preceding neonatal seizures caused by KCNQ2 R198Q, a gain-of-function variant. *Epilepsia* **58**, e10–e15 (2017).
57. E. Meisel, M. Dvir, Y. Haitin, M. Giladi, A. Peretz, B. Attali, KCNQ1 channels do not undergo concerted but sequential gating transitions in both the absence and the presence of KCNE1 protein. *J. Biol. Chem.* **287**, 34212–34224 (2012).
58. M. A. Zaydman, J. R. Silva, K. Delaloye, Y. Li, H. Liang, H. P. Larsson, J. Shi, J. Cui, Kv7.1 ion channels require a lipid to couple voltage sensing to pore opening. *Proc. Natl. Acad. Sci. U.S.A.* **110**, 13180–13185 (2013).
59. D. Ma, Y. Zheng, X. Li, X. Zhou, Z. Yang, Y. Zhang, L. Wang, W. Zhang, J. Fang, G. Zhao, P. Hou, F. Nan, W. Yang, N. Su, Z. Gao, J. Guo, Ligand activation mechanisms of human KCNQ2 channel. *Nat. Commun.* **14**, 6632 (2023).
60. T. Li, K. Wu, Z. Yue, Y. Wang, F. Zhang, H. Shen, Structural basis for the modulation of human KCNQ4 by small-molecule drugs. *Mol. Cell* **81**, 25–37.e4 (2021).
61. S. Zhang, D. Ma, K. Wang, Y. Li, Z. Yang, X. Li, J. Li, J. He, L. Mei, Y. Ye, Z. Chen, J. Shen, P. Hou, J. Guo, Q. Zhang, H. Yang, A small-molecule activation mechanism that directly opens the KCNQ2 channel. *Nat. Chem. Biol.* **20**, 847–856 (2024).
62. M. L. Chapman, H. M. VanDongen, A. M. VanDongen, Activation-dependent subconductance levels in the drk1 K channel suggest a subunit basis for ion permeation and gating. *Biophys. J.* **72**, 708–719 (1997).

63. M. L. Chapman, A. M. VanDongen, K channel subconductance levels result from heteromeric pore conformations. *J. Gen. Physiol.* **126**, 87–103 (2005).
64. G. Maksaev, M. Brundl-Jirout, A. Stary-Weinzinger, E. M. Zangerl-Plessl, S. J. Lee, C. G. Nichols, Subunit gating resulting from individual protonation events in Kir2 channels. *Nat. Commun.* **14**, 4538 (2023).
65. S. E. Dryer, Properties of single Na^+-activated K^+ channels in cultured central neurons of the chick embryo. *Neurosci. Lett.* **149**, 133–136 (1993).
66. A. Yuan, C. M. Santi, A. Wei, Z. W. Wang, K. Pollak, M. Nonet, L. Kaczmarek, C. M. Crowder, L. Salkoff, The sodium-activated potassium channel is encoded by a member of the Slo gene family. *Neuron* **37**, 765–773 (2003).
67. J. Sun, R. MacKinnon, Structural basis of human KCNQ1 modulation and gating. *Cell* **180**, 340–347.e9 (2020).
68. A. Alaimo, A. Villarroel, Calmodulin: A multitasking protein in Kv7.2 potassium channel functions. *Biomolecules* **8**, 57 (2018).
69. B. H. Falkenburger, J. B. Jensen, E. J. Dickson, B. C. Suh, B. Hille, Phosphoinositides: Lipid regulators of membrane proteins. *J. Physiol.* **588**, 3179–3185 (2010).
70. S. I. Liin, R. Barro-Soria, H. P. Larsson, The KCNQ1 channel – Remarkable flexibility in gating allows for functional versatility. *J. Physiol.* **593**, 2605–2615 (2015).
71. E. Thompson, J. Eldstrom, M. Westhoff, D. McAfee, E. Balse, D. Fedida, cAMP-dependent regulation of I_{KS} single-channel kinetics. *J. Gen. Physiol.* **149**, 781–798 (2017).
72. E. Thompson, J. Eldstrom, D. Fedida, Hormonal signaling actions on Kv7.1 (KCNQ1) channels. *Annu. Rev. Pharmacol. Toxicol.* **61**, 381–400 (2021).
73. H. Soh, K. Springer, K. Doci, J. L. Balsbaugh, A. V. Tzingounis, KCNQ2 and KCNQ5 form heteromeric channels independent of KCNQ3. *Proc. Natl. Acad. Sci. U.S.A.* **119**, e2117640119 (2022).
74. L. Backwell, J. A. Marsh, Diverse molecular mechanisms underlying pathogenic protein mutations: Beyond the loss-of-function paradigm. *Annu. Rev. Genomics Hum. Genet.* **23**, 475–498 (2022).
75. L. T. Bergendahl, L. Gerasimavicius, J. Miles, L. Macdonald, J. N. Wells, J. P. I. Welburn, J. A. Marsh, The role of protein complexes in human genetic disease. *Protein Sci.* **28**, 1400–1411 (2019).
76. Y. Geng, P. Li, A. Butler, B. Wang, L. Salkoff, K. L. Magleby, BK channels of five different subunit combinations underlie the de novo KCNMA1 G375R channelopathy. *J. Gen. Physiol.* **155**, e202213302 (2023).
77. R. Barro-Soria, Epilepsy-associated mutations in the voltage sensor of KCNQ3 affect voltage dependence of channel opening. *J. Gen. Physiol.* **151**, 247–257 (2019).
78. C. I. Murray, M. Westhoff, J. Eldstrom, E. Thompson, R. Emes, D. Fedida, Unnatural amino acid photo-crosslinking of the IKs channel complex demonstrates a KCNE1:KCNQ1 stoichiometry of up to 4:4. *eLife* **5**, e11815 (2016).
79. M. Westhoff, C. I. Murray, J. Eldstrom, D. Fedida, Photo-cross-linking of I_{KS} demonstrates state-dependent interactions between KCNE1 and KCNQ1. *Biophys. J.* **113**, 415–425 (2017).
80. J. D'Errico, fminsearchbnd, fminsearchcon (MATLAB Central File Exchange, 2024).
81. J. A. Nelder, R. Mead, A simplex method for function minimization. *Comput. J.* **7**, 308–313 (1965).
82. J. D. Moreno, T. J. Lewis, C. E. Clancy, Parameterization for in-silico modeling of ion channel interactions with drugs. *PLOS ONE* **11**, e0150761 (2016).

Acknowledgments: We thank F. Ataei for technical assistance with cell culture and cloning. **Funding:** This work was supported by the National Institutes of Health (1R01NS110847) to R.B.-S. and the Natural Sciences and Engineering Research Council of Canada (grant no. RGPIN-2022-03021), the Canadian Institutes of Health Research (grant no. PJT-175024), and the Heart and Stroke Foundation of Canada (grant no. G-21-0031566) to D.F. **Author contributions:** Conceptualization: J.E., D.F., and R.B.-S. Methodology: A.H.-P., J.E., A.M.-A., M.A.E., A.d.l.C., M.E.P.R., M.D.-S., D.M.D., D.F., and R.B.-S. Investigation: A.H.-P., J.E., Y.D., A.M.-A., M.A.E., A.d.l.C., M.E.P.R., M.D.-S., D.F., and R.B.-S. Visualization: A.H.-P., J.E., M.A.E., A.d.l.C, M.E.P.R., M.D.-S., D.F., and R.B.-S. Formal analysis: A.H.-P., J.E., A.M.-A., M.A.E., A.d.l.C., M.E.P.R., M.D.-S., D.F., and R.B.-S. Validation: A.H.-P., J.E., A.M.-A., M.A.E., A.d.l.C., D.F., and R.B.-S. Resources: D.M.D., D.F., and R.B.-S. Project administration: J.E., M.E.P.R, D.F., and R.B.-S. Funding acquisition: D.F. and R.B.-S. Software: D.F. and R.B.-S. Data curation: J.E., D.M.D., D.F., and R.B.-S. Supervision: J.E., D.F., and R.B.-S. Writing—original draft: A.H.-P., J.E., D.M.D., D.F., and R.B.-S. Writing—review and editing: J.E., D.F., and R.B.-S. **Competing interest:** The authors declare that they have no competing interests. **Data and materials availability:** All data needed to evaluate the conclusions in the paper are present in the paper and/or the Supplementary Materials.

Submitted 13 July 2024
Accepted 29 January 2025
Published 5 March 2025
10.1126/sciadv.adr7012